Arabidopsis CNL receptor SUT1 confers immunity in hydathodes against the vascular pathogen *Xanthomonas campestris* pv. *campestris*

Short title:

SUT1 confers immunity to Xcc in Arabidopsis hydathodes

Author list:

Nanne W. Taks[1], Marieke van Hulten[1], Jeroen A. van Splunter-Berg[1], Sayantani Chatterjee[1], Floris D. Stevens[1], Misha Paauw[1], Sebastian Pfeilmeier[1] and Harrold A. van den Burg[1,2]

1) Molecular Plant Pathology, Swammerdam Institute for Life Sciences, Faculty of Science, University of Amsterdam, Science Park 904, 1098 XH, Amsterdam, the Netherlands
2) Rijk Zwaan Zaadteelt en Zaadhandel B.V., Burgemeester Crezéelaan 40, 2678 ZG, De Lier, The Netherlands

***Author for correspondence:** H.A. van den Burg

Email: H.A.vandenBurg@uva.nl, Tel +31 20 525 7797

Figures: 5

Supporting figures: 7

Supporting tables: 1

Extended data files: 2

Abstract (290 words)

Bacterial plant pathogens exploit natural openings, such as pores or wounds, to enter the plant interior and cause disease. Plants guard these openings through defense mechanisms. However, bacteria from the genus *Xanthomonas* have specialized in that they enter their host via a special entry point, the hydathode—an organ at the leaf margin involved in xylem sap guttation. Hydathodes can mount an immune response against bacteria, including non-adapted and adapted pathogens like *X. campestris* pv. *campestris* (Xcc) that cause vascular disease. Previously, it was shown that the RKS1/ZAR1 immune complex confers vascular resistance against Xcc by recognizing XopAC activity, a type III effector (T3E). However, in absence of XopAC recognition, Arabidopsis Col-0 hydathodes still display resistance against Xcc. Here we mapped the causal gene using an inoculation method that promotes Xcc hydathode entry. Using a population of Recombinant Inbred Lines (RILs) of a cross between a susceptible (Oy-0) and resistant accession (Col-0), a major QTL for Xcc resistance was found on the right arm of Chromosome 5 in Col-0. Combining this result with a genome-wide association analysis yielded a single candidate gene encoding a coiled-coil nucleotide-binding leucine-rich repeat (CNL-type) immune receptor protein called SUPPRESSOR OF TOPP4 1 (SUT1). Expression of *SUT1* was confirmed in hydathodes. We reveal that RKS1/ZAR1 and SUT1 confer different levels of Xcc resistance in different tissue types. Both RKS1/ZAR1 and SUT1 are alone sufficient for Xcc resistance in Col-0 hydathodes. However, RKS1/ZAR1 resistance is also effective in tissue types that represent late infection stages, i.e. xylem and mesophyll. In contrast, SUT1 resistance is not effective in the xylem, while weakly additive to RKS1/ZAR1 in the mesophyll. We thus identify a novel *R* gene, *SUT1*, that confers Xcc resistance primarily early in the infection during hydathode colonization.

Author summary

Black rot disease, caused by the bacterial pathogen *Xanthomonas campestris* pv. *campestris* (Xcc), is an economically important disease of cabbage crops. Xcc is unique in that it enters the plant interior through specialized organs at the leaf margin. These structures called hydathodes contain water pores and are involved in root pressure regulation. Although we know that hydathodes can mount an immune response against these bacteria, specific immune receptors still need to be discovered. Here we use the model plant *Arabidopsis thaliana* to map an hydathode-effective resistance gene. By screening two different Arabidopsis populations, we could map a single gene, *SUT1,* that is involved in this resistance. SUT1 restricts the early hydathode colonization by Xcc thus suppressing disease progression. Interestingly, SUT1 resistance was not effective in the plant vascular system, which the bacteria subsequently colonize. Therefore, this study provides a new insight into the role of hydathodes in anti-bacterial resistance in plants and opens the door for research on tissue- and organ-specific resistance mechanisms.

58 **Introduction**

59 Plant pathogenic microbes employ different strategies to invade their host and induce disease.
60 Foliar bacterial pathogens primarily exploit natural openings of plants, such as pores involved in
61 gas exchange (stomata) or in water and nutrient homeostasis (hydathodes). Consequently,
62 plants have evolved a plethora of immune mechanisms to guard these openings and to respond
63 to invading pathogens [1,2]. Among these entry points, stomata are arguably the best studied in
64 the context of plant immunity. Several immune mechanisms have been elucidated, including the
65 sensing of microbe-associated molecular patterns (MAMPs), such as bacterial flagellin [3] or
66 fungal chitin [4]. Upon perception, plants activate a signaling cascade that includes pre-invasive
67 closure of the stomatal pores followed by post-invasive opening [5–7]. While stomata provide
68 access to the leaf apoplast, hydathodes represent an entry point for highly specialized bacterial
69 pathogens that colonize the leaf vasculature [8–10]. The hydathode anatomy is composed of an
70 enclosed extracellular cavity interspersed with small mesophyll-like epithem cells. The cavity is
71 connected to the exterior via stomata-like openings in the epidermis called water pores [11,12].
72 Water pores allow xylem sap exudation, a process known as guttation, in conditions when the
73 root pressure exceeds water evaporation by transpiration [13]. The cavity is connected to endings
74 of the xylem trachea. The epithem tissue appears to act as an active filter of the guttation fluid,
75 reabsorbing salts and nutrients prior to extrusion [13]. Interestingly, the water pores do not
76 completely close in response to pathogens [8,14], providing nearly unrestricted access to the
77 hydathode cavity. Several pathogenic *Xanthomonas* spp. are known to invade their hosts via
78 hydathodes [8,9,15]. Despite the absence of pre-invasive immunity, a post-invasive immune
79 response is mounted in hydathodes against hydathode-adapted and non-adapted bacterial
80 pathogens [16], which restricts bacterial proliferation in the hydathode cavity and thereby
81 reduces the number of vascular outbreaks. Intriguingly, although general immune signaling hubs
82 have been confirmed to be involved in this hydathode immune response, knowledge on immune
83 receptors that act in hydathodes remains limited.

84 Plant immune receptors can be classified as cell-surface and intracellular receptors [17,18].
85 While cell-surface pattern recognition receptors (PRRs) generally detect well-conserved
86 microbe-associated molecular patterns (MAMPs), intracellular nucleotide-binding leucine-rich
87 repeat (NLR) receptors respond directly or indirectly to the mode of action of pathogen-derived
88 effector proteins. These effectors promote virulence upon delivery into the host cell to
89 manipulate cellular processes including plant immunity [19]. Plant NLRs can be subdivided into
90 three groups based on their N-terminal domain, that is, Coiled-coil (CC) NLRs (CNLs),
91 Toll/Interleukin-1 receptor/Resistance (TIR) NLRs (TNLs), and RPW8-like CC domain (RPW8)
92 helper NLRs (RNLs) [20]. While some NLRs activate immune responses by themselves through
93 oligomerization into a so-called resistosome complex [21], others rely on helper NLRs or are part
94 of an NLR network that triggers immune signaling [18]. The evolution of plant immune receptor
95 networks and pathogen immune suppressors has shaped the landscape of most plant-pathogen
96 interactions [17].

97 Both plant immune receptors and pathogen effectors have been studied extensively in
98 *Arabidopsis thaliana* (hereafter Arabidopsis), in particular using the stomata-invading bacterium
99 *Pseudomonas syringae* [22]. For hydathode-infecting bacteria, such as *Xanthomonas campestris*
100 pv. *campestris* (Xcc) [10], only a few resistance mechanisms have been studied. For example, the
101 RESISTANCE RELATED KINASE 1 (RKS1)/HOPZ-ACTIVATED RESISTANCE (ZAR1) immune complex
102 recognizes uridylation of the pseudokinase PBL2 by the Xcc effector XopAC (AvrAC) [23,24]. This
103 immune complex confers resistance to Xcc already in hydathodes [8,16] as well as later during
104 the infection when the bacteria spread systemically along the xylem vessels [24] and eventually
105 breakout towards the mesophyll [25]. However, many Arabidopsis accessions, including Col-0,
106 still display a considerable level of resistance in hydathodes against Xcc strains that lack *xopAC*
107 [16], indicating that additional pathogen perception mechanism are present in these accessions.

108 This notion is corroborated by the fact that plant lines lacking the PRR co-receptors BRI1-
109 ASSOCIATED RECEPTOR KINASE 1 (BAK1) and its close homolog BKK1 (BAK1-LIKE 1, SERK4) are
110 more susceptible to hydathode colonization by bacterial pathogens [16]. In addition, the immune
111 signaling hub formed by the proteins ENHANCED DISEASE SUSCEPTIBILITY 1 (EDS1) –
112 PHYTOALEXIN DEFICIENT 4 (PAD4) – ACTIVATED DISEASE RESISTANCE 1 (ADR1) was shown to
113 be needed for restricting hydathode colonization by Xcc [16]. Hence, it becomes apparent that
114 another effective, post-invasive immune response exists in Arabidopsis Col-0 against adapted
115 bacteria in hydathodes, yet the causal receptor for this immune recognition remains elusive. To
116 fill this knowledge gap on hydathode immunity, we set out to identify the causal resistance gene.

117 **Results**

118 **A QTL on Chromosome 5 is associated with resistance against Xcc *ΔxopAC***

119 Earlier, we showed that the Arabidopsis accession Col-0 shows a high level of resistance to the
120 vascular bacterial pathogen Xcc8004 in guttation-based infections and that this response was
121 independent of XopAC recognition by RKS1/ZAR1 [16]. Furthermore, the same study showed that
122 the accession Oy-0 is susceptible to the same mutant bacterial strain (Xcc8004 *ΔxopAC*),
123 meaning that we can use a segregating population between Oy-0 × Col-0 to map the causal
124 gene(s) for this resistance. To this end, we made use of an existing Arabidopsis population of
125 Recombinant Inbred Lines (RILs) between Oy-0 × Col-0, composed of 470 RILs [26]. In total, we
126 screened for resistance in 165 RILs of this population that showed the most complete annotation
127 of markers to the parental genomes, including the two parental lines Oy-0 and Col-0, using a
128 bioluminescent reporter strain (Tn*5*:*lux*) of Xcc8004 *ΔxopAC* [16,27]. For each plant, the three
129 most symptomatic leaves were sampled 14 days post inoculation (dpi) and bacterial colonization
130 was visualized using light-sensitive films (Figure 1A). The level of resistance was then scored
131 using a luminescence index ordinal scale [27] and normalized to the Oy-0 control for each
132 experiment (Figure 1B and C). Using an Expectation-maximization (EM) model for a single QTL

133 [28] and LOD threshold set at 2.49 by permutation (n = 1000), three QTLs were identified, that is,

134 one at Chromosome 4 and two on Chromosome 5 (Figure 1D). These QTLs showed an explained

135 variance (EV) of 10, 11 and 32%, respectively. The major QTL at the end of the right arm of

136 Chromosome 5 had an LOD score of 14.92 and thus displayed a strong genetic association with

137 the resistance phenotype in the Oy-0 × Col-0 RIL population.

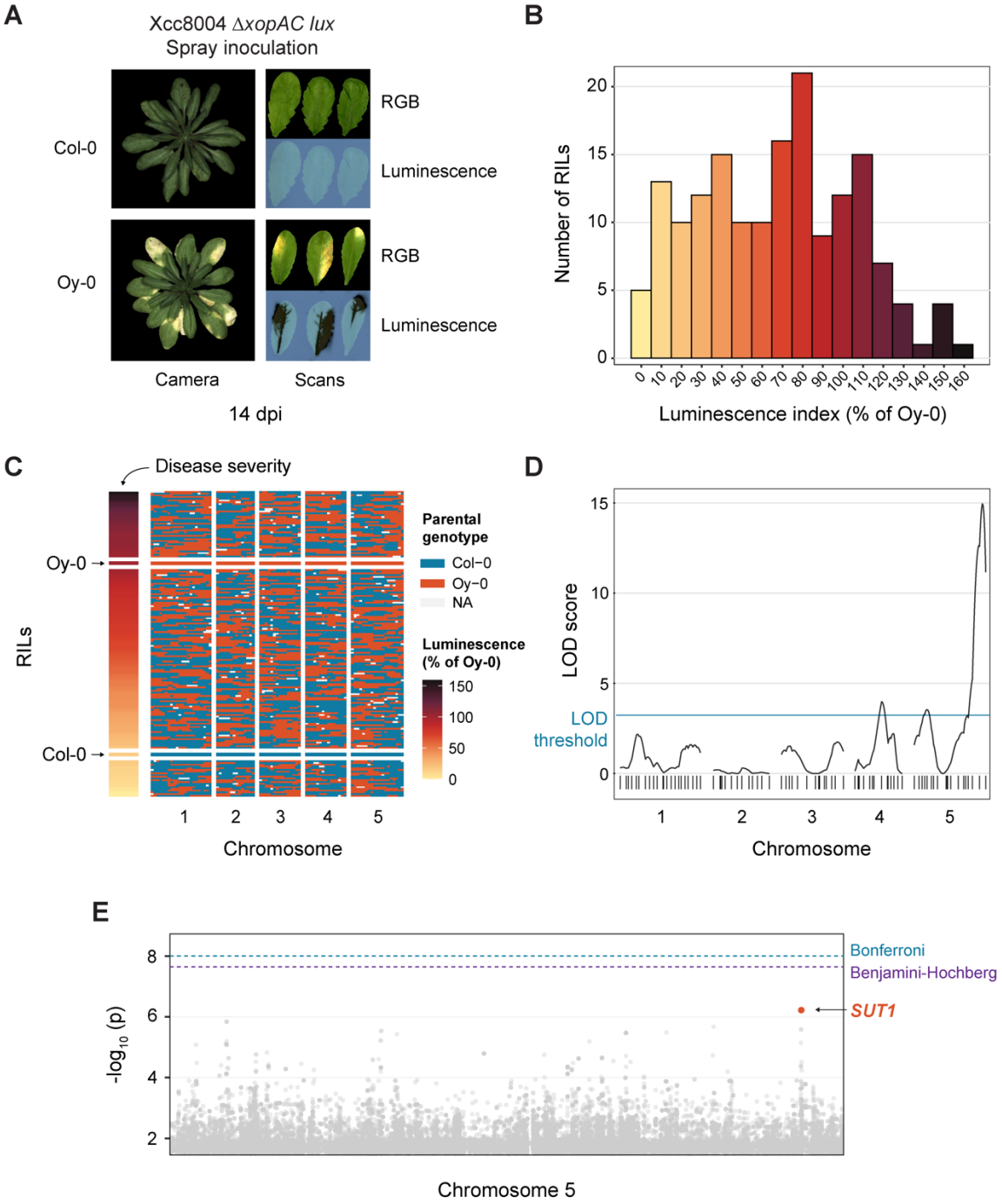

138

Figure 1. Mapping of *SUT1* as a candidate *R* gene against Xcc8004 *ΔxopAC* in Arabidopsis Col-0. A) Disease symptoms and bacterial luminescence in the resistant Col-0 and susceptible Oy-0 accessions following spray inoculation with bioluminescent Xcc8004 *ΔxopAC*. Leaves shown are representative of spray inoculation with either Tn*5:lux* or Tn*7:lux* tagged reporter strains. Bacterial spread was visualized using light-sensitive film 14 days post inoculation (dpi). **B)** Histogram depicting the variation in luminescence index score 14 dpi (normalized to Oy-0) for all 165 Oy-0 × Col-0 Recombinant Inbred Lines (RILs) following spray inoculation with Xcc8004 *ΔxopAC* Tn*5:lux*. **C)** Population structure of 165 RILs in the Oy-0 × Col-0 RIL population, ordered by luminescence index score at 14 dpi (normalized to Oy-0) shown in (B). **D)** QTL graph showing LOD scores for each of the 85 markers in the RIL population. LOD significance threshold determined by permutation (n = 1000) at 2.49 **E)** Manhattan plot of Chromosome 5 from a screen of 321 accessions present in the HapMap collection. Highlighted SNPs in orange are located within the coding sequence of *SUT1*. False Discovery Rate (FDR) thresholds set at $-\log_{10}$ (p) = 8 (Bonferroni) and $-\log_{10}$ (p) = 7.29 (Benjamini-Hochberg). See also Figure S1 for the full Manhattan plot.

Genome-wide association study (GWAS) identified candidate *R* gene *SUT1*

To identify candidate genes in the major QTL on Chromosome 5, a GWAS was performed with the same Xcc8004 *ΔxopAC* Tn*5:lux* reporter strain on the Arabidopsis HapMap population [29]. In total 321 accessions from this populations were evaluated for Xcc disease susceptibility 14 dpi and the data obtained was normalized to the Oy-0 control to control for batch effects. GWA analysis was performed on phenotypic data using an online GWA portal, based on an imputed SNP dataset of over five million SNPs [30]. Unexpectedly, no SNPs were identified with a significant correlation to the disease phenotype on Chromosome 5 (Figure 1E and S1). However, several SNPs that were close to the False Discovery Rate (FDR)-corrected significance threshold coincided with the major QTL (Figure 1E), suggesting an association with the Col-0 disease resistance. These SNPs were located in the coding sequence of the gene At5g63020, which codes for SUPPRESSOR OF TOPP4 (SUT1), a previously characterized CNL involved in plant immunity [31].

165 **SUT1 is involved in hydathode resistance against Xcc**

166 To further investigate the role of SUT1 in plant immunity in Col-0 and Oy-0, we aligned the
167 respective *SUT1* alleles using recently published whole genome assemblies of the two
168 accessions [32] and confirmed them by Sanger sequencing of the Col-0 and Oy-0 accessions
169 used in our laboratory. The sequence alignment identified SNPs in the $SUT1^{Oy\text{-}0}$ coding sequence
170 including six non-synonymous changes that result in amino acid substitution (Figure 2A and S2).
171 In addition, one single base insertion leads to a frameshift and a predicted three-residue peptide
172 extension of $SUT1^{Oy\text{-}0}$. All but one of the predicted amino acid changes are in the leucine-rich
173 repeat (LRR) domain, which is known to act as a protein-protein interaction surface [33] for target
174 sensing and ligand binding [21,34]. These sequence differences between $SUT1^{Col\text{-}0}$ and $SUT1^{Oy\text{-}0}$
175 could thus explain the difference in Xcc disease resistance between Oy-0 and Col-0

176 To assess if a *SUT1* null allele in Col-0 would lead to loss-of-resistance, two known *sut1* T-DNA
177 insertion mutants, *sut1-8* and *sut1-9,* were tested for increased Xcc disease susceptibility (Figure
178 2B). Previously, these two T-DNA insertion lines were shown to result in recovery of the *topp4-1*
179 dominant autoimmune phenotype [31], implying that SUT1 is no longer functional in both
180 mutants. To confirm a role of SUT1 in Xcc resistance, both mutants were spray inoculated with
181 Xcc8004 *ΔxopAC* Tn*7:lux* and the level of resistance was assessed both early in the infection in
182 hydathodes (7 dpi) and at late stages during leaf colonization (14 dpi). Compared to the wildtype
183 Col-0 control, both *sut1-8* and *sut1-9* showed an increased number of severe hydathode
184 infections at 7 dpi (Figure 2C and D), and enhanced leaf chlorosis (Figure 2C and E) combined
185 with increased bacterial spread at 14 dpi (Figure 2C and F). During the early stage of hydathode
186 colonization, the *sut1* mutants showed an intermediate level of susceptibility in comparison to
187 the susceptible controls (i) *bak1-5;bkk1-1* (*bb*) in the Col-0 background and (ii) the susceptible
188 accession Oy-0. Furthermore, disease symptom development was more severe in the Oy-0
189 plants than in the *sut1* knockout lines, which is consistent with the fact that two minor QTLs with

190 a significant LOD score were found in the RIL population as well (Figure 1D). Possibly, these two
191 loci are as well involved in disease resistance besides *SUT1* in Col-0. A previous study showed
192 that SUT1 is needed for dominant autoimmune phenotype in the Col-0 mutant background
193 caused by a specific protein variant of the TYPE 1 PROTEIN PHOPSHATASE 4 (TOPP4), suggesting
194 that the NLR SUT1 guards the TOPP4 protein activity [31]. To infer if TOPP4 itself is also important
195 for Xcc resistance in Col-0, a previously characterized *topp4* knockout line was inoculated with
196 Xcc8004 *ΔxopAC* Tn*7:lux*. A minor but significant increase in the number of infected hydathodes
197 was seen in the *topp4* knockout line, but no increase was seen in bacterial spread across the leaf
198 or leaf chlorosis during later infection stages (Figure S3). Apparently, SUT1 immunity to Xcc does
199 not depend one-on-one on guarding TOPP4. Future work should reveal whether other TOPP family
200 members have a role in SUT1 resistance against Xcc. We thus conclude that SUT1 restricts Xcc
201 proliferation inside hydathodes, thereby reducing both Black rot disease symptom development
202 and the systemic spread of Xcc along the leaf vasculature.

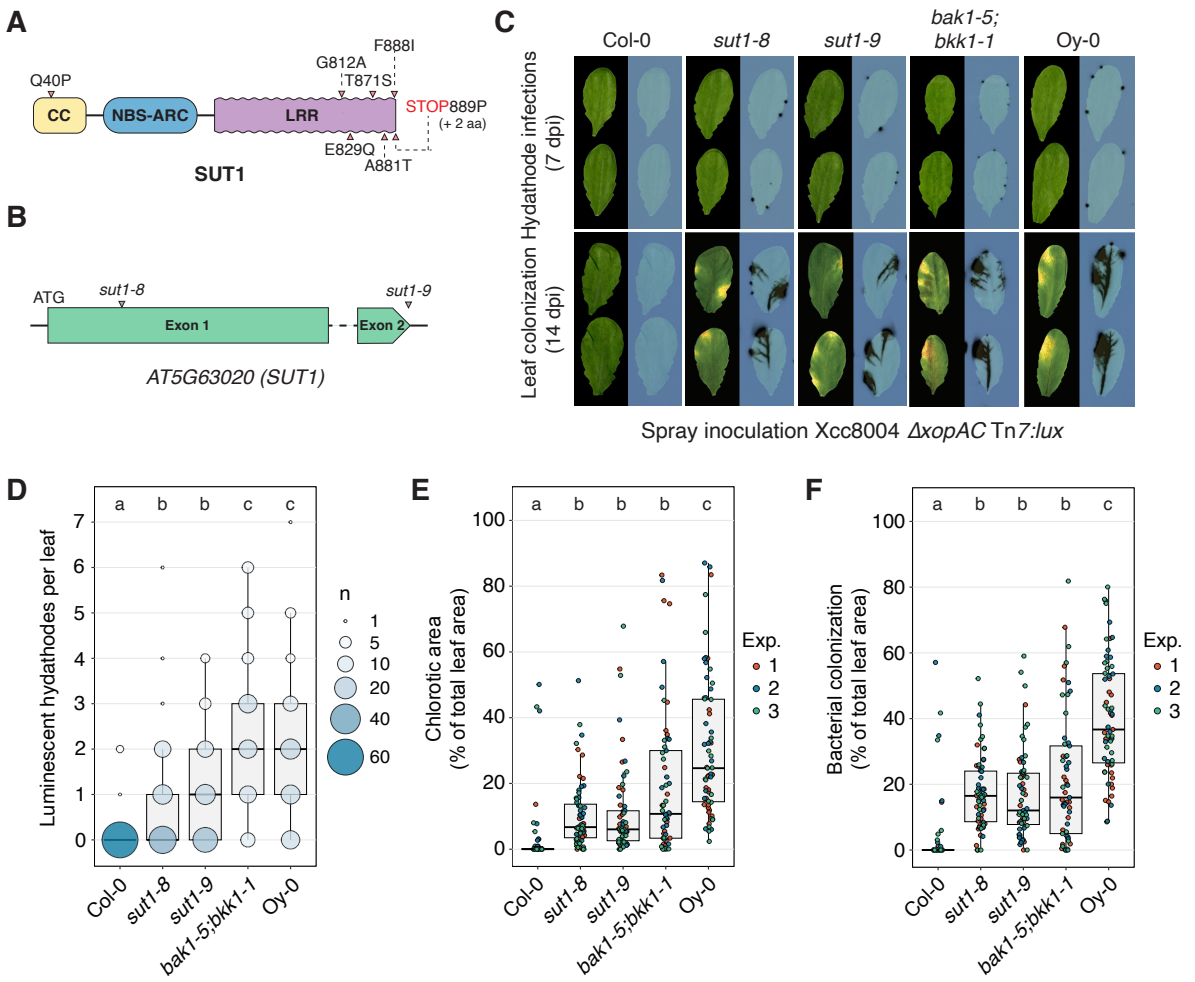

Figure 2. SUT1 contributes to hydathode resistance against Xcc8004 *ΔxopAC*. A) Predicted SUT1 protein model. Arrows depict predicted amino acid differences between Oy-0 vs. Col-0. **B)** *SUT1* gene model depicting the Col-0 allele and approximate integration site of the *sut1-8* and *sut1-9* T-DNA insertions. **C)** Spray inoculation of *sut1-8* and *sut1-9* with Xcc8004 *ΔxopAC* Tn*7:lux*. Wildtype background (Col-0), *bak1-5;bkk1-1* (Col-0) and the accession Oy-0 were included as controls. *Top,* visualization of high density hydathode colonization using light sensitive films (7 dpi); *bottom*, visualization of the systemic spread of Xcc and disease symptom development (14 dpi). **D,E,F)** Number of infected hydathodes 7 dpi (**D**), chlorotic area 14 dpi (**E**) and bacterial colonization 14 dpi (**F**) per leaf for each line shown in panel C following spray inoculation with Xcc8004 *ΔxopAC* Tn*7:lux* (n = 21 leaves per experiment). In panel D, the circle size depicts the number (#) of leaves with a certain score (y-axis) from three independent repetitions. Significance letters from non-parametric Kruskal-Wallis test with Dunn's Post-Hoc test, p-value threshold = 0.05.

214 ***SUT1* is expressed in different cell types including the epithem**

215 As SUT1 confers resistance already in the hydathodes, we hypothesized that the *SUT1* gene is
216 expressed in the hydathode epithem cells. To further investigate this idea, transgenic reporter
217 lines were generated that express the *β-glucuronidase (GUS*) reporter gene from the *SUT1*
218 promoter using the 2.1 kb DNA fragment upstream of the *SUT1* start codon for histochemical
219 staining of whole leaves. GUS straining was detected in the entire leaf of 4-week-old T1 transgenic
220 plants with a more intense blue staining of the hydathodes (Figure 3A and S4). As others reported
221 earlier that GUS staining of hydathodes can be the result of false positive staining [35], an
222 independent reporter system was generated as well that gives YFP fluorescence in nuclei,
223 *pSUT1::NLS-3×mVENUS* [36]. As a reference for epithem cells, we used our epithem marker line
224 *pPUP1::RCl2A-tdTomato* [16], which displays red fluorescence at the epithem cell membrane
225 (Figure 3B). Col-0 plants expressing *pSUT1::NLS-3×mVENUS* showed a fluorescent YFP signal
226 both in the nuclei of epithem cells and throughout the mesophyll tissue (Figure 3C and S5). These
227 findings are supported by several studies on single-cell transcriptomics that indicate expression
228 of *SUT1* in different cell types [37], including the mesophyll and epithem [13,38]. Taken together,
229 these data confirm *SUT1* expression in the epithem cells within hydathodes.

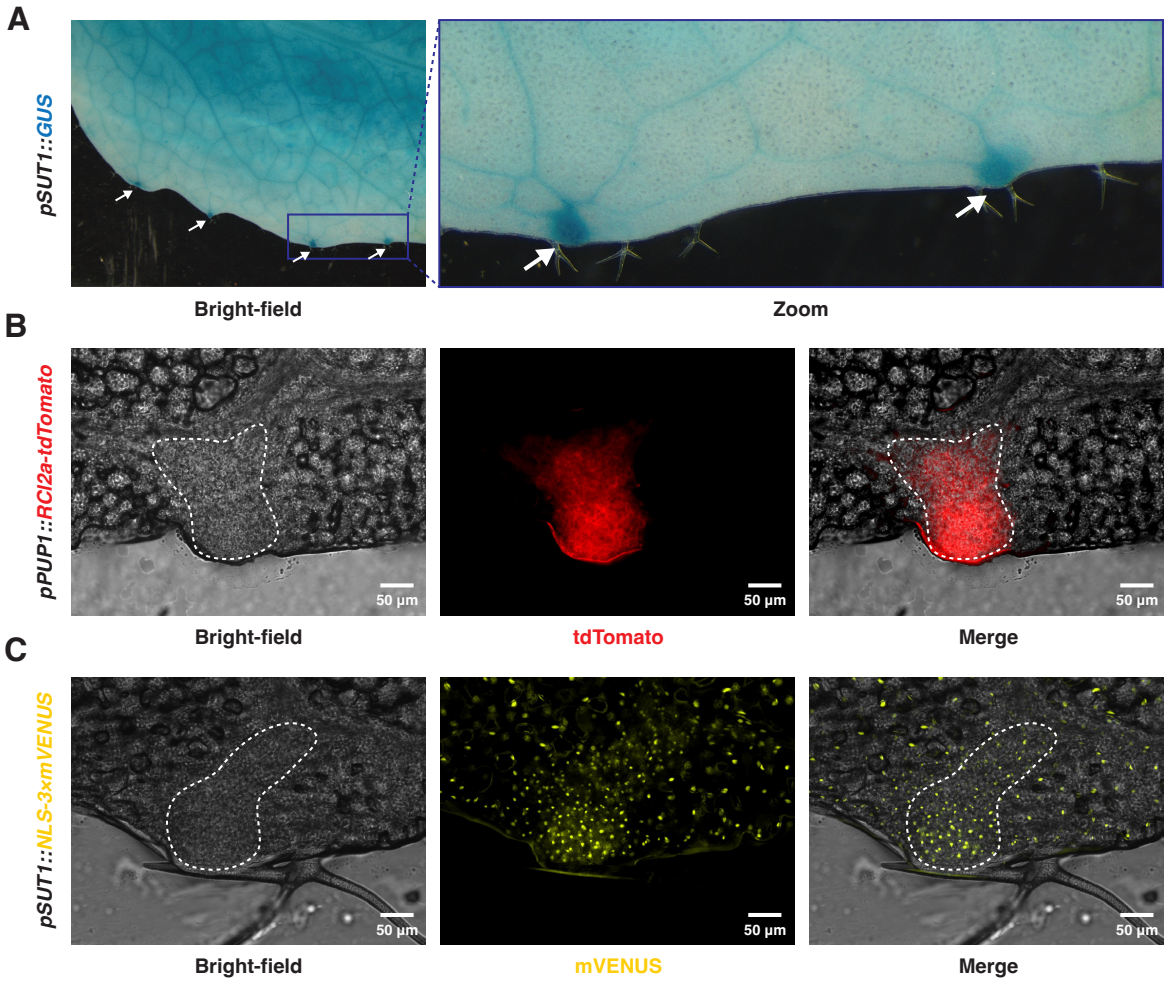

Figure 3. *SUT1* is expressed in epithem cells within hydathodes. A) Arabidopsis *pSUT1::GUS* lines stained with X-Gluc show *SUT1* expression over the entire leaf (4-week-old plants). GUS staining is stronger in the hydathodes along the leaf margin (white arrows). **B)** Arabidopsis epithem marker line *pPUP1::RCl2a-tdTomato* shows tdTomato localization in epithem cell membrane within hydathodes. Epithem tissue can be distinguished from the mesophyll cells in the bright-field image (white dashed line). **C)** Arabidopsis *pSUT1::NLS3×mVENUS* T_2 line shows mVENUS accumulation in nuclei of mesophyll and epithem cells. Epithem cells can be distinguished from mesophyll cells in the bright-field image as a region with dense small cells on the leaf margin (white dashed line). Images were taken of epidermal peels and are representative of three independent lines (Figure S5).

239 **SUT1-mediated resistance is ineffective when hydathodes are bypassed**

240 As SUT1 already provides resistance to Xcc already during the first stage of infection, we
241 wondered whether SUT1 also contributes to resistance (a) at later stages of the infection or (b)
242 upon wound inoculation when the bacteria invade the leaf vasculature. To this end, clipping
243 inoculations were performed to provide the bacteria direct access to the midvein and lateral veins
244 near the leaf apex, thereby bypassing the hydathodes. We quantified both the bacterial spread
245 along the midvein and the relative chlorotic leaf area (as a proxy of disease symptom
246 development) (Figure 4A). Strikingly, SUT1 resistance was lost when the hydathodes were
247 bypassed. First, we found no difference in the leaf chlorosis between the *sut1* mutants and the
248 wildtype control (Figure 4B). Second, the total distance that the bacteria can progress along the
249 midvein was apparently also unaffected in *sut1-9* compared to the wildtype control Col-0 (Figure
250 4C). This tissue-specific response differs to RKS1/ZAR1 immunity that is also effective in the
251 vasculature, as shown by clipping inoculation of Xcc8004 WT Tn*5:lux* in Col-0 and both *rks1-1* and
252 *zar1-1* knockout lines (Figure S6); others reported earlier a similar finding when Xcc was
253 introduced into the midvein by pin inoculations [24,39]. Overall, these results indicate that
254 RKS1/ZAR1 and SUT1 display a different resistance level against an Xcc infection in the different
255 tissue types.

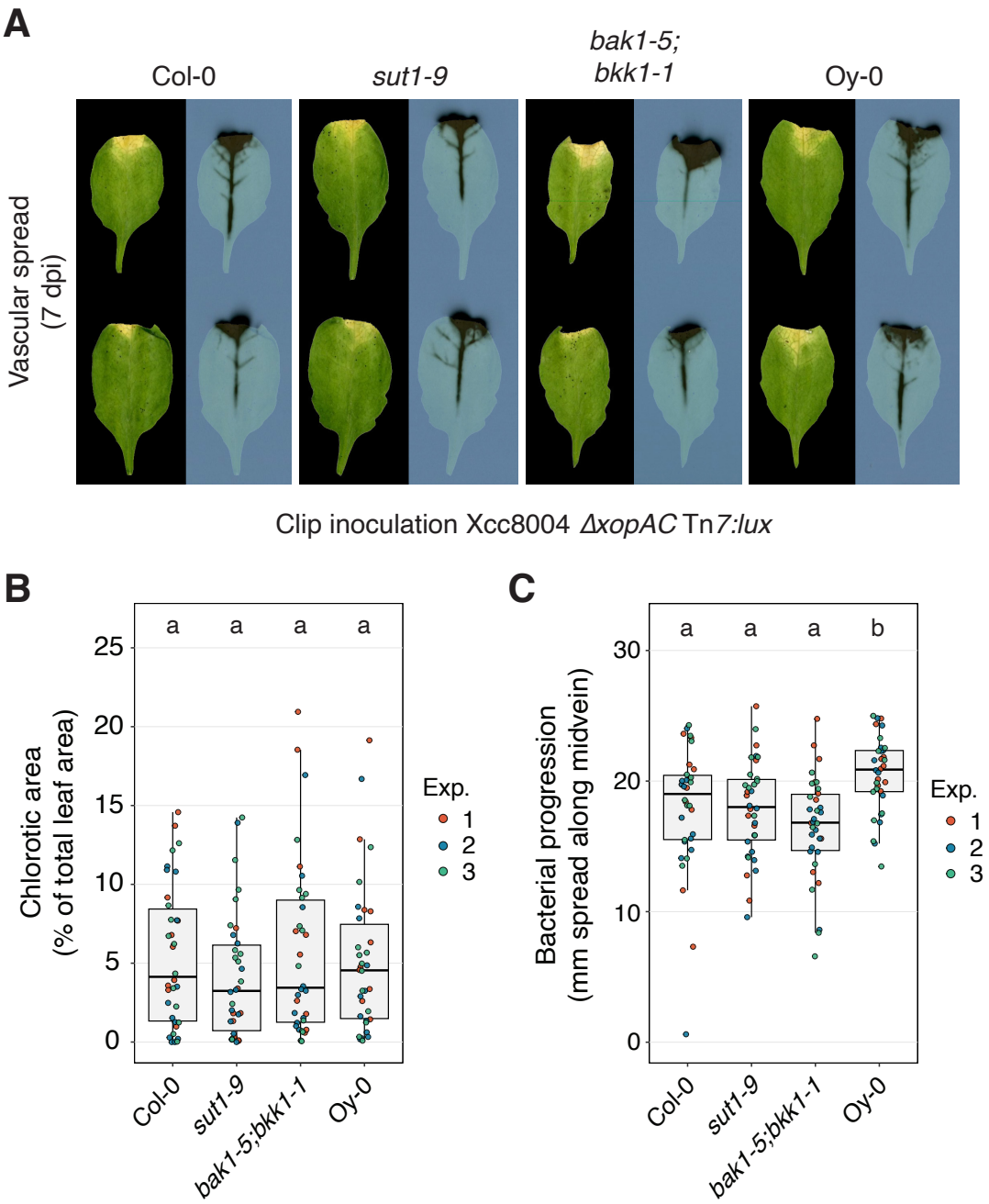

Figure 4. SUT1 resistance is compromised when the Xcc inoculation bypasses hydathode colonization. A) Disease symptoms and bacterial spread in Col-0, *sut1-9*, *bak1-1;bkk1-5* and Oy-0 leaves at 7 dpi following clip inoculation with Xcc8004 *ΔxopAC* Tn*7:lux*. Bacterial progression is quantified as the spread of the luminescence signal along the midvein. **B,C)** Chlorotic leaf area (**B**) and bacterial spread along the midvein (**C**) 7 dpi following clip inoculation with Xcc8004 *ΔxopAC* Tn*7:lux*. SUT1 resistance against Xcc is apparently ineffective in the vasculature of Col-0 when the hydathodes are bypassed and the bacteria are introduced using leaf clipping. Significance letters from a two-way ANOVA with Tukey Post-Hoc test, p-value threshold = 0.05 (n = 12 leaves per experiment).

263 ***RKS1/ZAR1* and *SUT1* confer effective resistance in different plant tissues**

264 As we detected *SUT1* expression throughout the leaf, but no effective *SUT1* resistance outside
265 hydathodes, we further examined if *RKS1/ZAR1* and *SUT1* confer additive resistance in the
266 different plant tissues. To this end, r*ks1/sut1* double knockout mutants were generated in
267 Arabidopsis Col-0 using the CRISPR/zCas9i toolkit [40] (Figure S7). Next, we evaluate the
268 resistance level that *RKS1/ZAR1* and *SUT1* provide at different stages of the infection using the
269 wildtype strain Xcc8004 Tn*7:lux* strain. To this end, three different inoculation methods were
270 used, that is, spray inoculations (entry via hydathodes), clip inoculations (to access xylem
271 vessels) and syringe infiltrations (to provide direct access to the mesophyll). Resistance against
272 Xcc was examined in the wildtype Arabidopsis Col-0 (with functional *RKS1/ZAR1* and *SUT1*),
273 plants defective for one of two *R* genes (i.e. *rks1-1* and *sut1-9*) and plants defective in both (i.e.
274 *rks1/sut1* and Oy-0). As Oy-0 is known to be susceptible to Xcc8004 secreting T3E XopAC [16], we
275 assumed that this accession lacks both a functional *RKS1/ZAR1* and *SUT1*. In spray inoculation
276 experiments that mimic natural infection, we found the *rks1-1* and *sut1-9* single mutants
277 displayed a similar level of resistance against Xcc, both in hydathodes (Figure 5A and B, 7 dpi)
278 and when the bacteria were spreading along the leaf vasculature (Figure 5A and C, 14 dpi).
279 Therefore, *RKS1/ZAR1* and *SUT1* independently confer resistance in the hydathodes thereby
280 reducing Xcc outbreak towards the xylem. The *rks1/sut1* double mutants showed a similar level
281 of susceptibility as the Oy-0 control, indicating that *RKS1/ZAR1* and *SUT1* together represent the
282 main resistance genes in Col-0 that halt Xcc in the initial phase of the infection.

283 When the bacteria were directly introduced into the xylem vessels by clipping, it was noted that
284 *RKS1/ZAR1* effectively prevented Xcc vascular spread (Figure 5D and E). In contrast, *SUT1*
285 resistance appears not to act in the xylem, as the *rks1-1* plants showed a similar vascular spread
286 as the *rks1/sut1* double mutants and the Oy-0 control (Figure 5D and E), confirming our earlier
287 observations (Figure 4). Therefore, *RKS1/ZAR1* is effective in halting an Xcc infection even when

288 the hydathodes are bypassed, whereas *SUT1* is not. To further assess the resistance level at the
289 late infection stage when Xcc spreads into the mesophyll tissue, direct mesophyll inoculations
290 were performed using syringe infiltrations. Plants expressing a functional *RKS1/ZAR1* showed a
291 strong reduction in bacterial proliferation compared to Oy-0 (Figure 5F). Similar to the xylem
292 vessels, we found that the *rks1-1* plants showed significantly more Xcc bacterial proliferation than
293 the *sut1-9* plants, indicating that *RKS1/ZAR1* resistance is also the main source of resistance in
294 the Col-0 mesophyll. In corroboration, at 5 dpi the *rks1/sut1* double mutants displayed a small
295 yet significant increase in Xcc proliferation compared to the *rks1-1* single mutant, suggesting that
296 SUT1 has a minor additive effect on plant immunity in the Col-0 mesophyll against Xcc (Figure
297 5F). Altogether, these results indicate a differential immune response by *RKS1/ZAR1* and *SUT1* to
298 Xcc infections in different tissue types, as *RKS1/ZAR1* confers resistance in all tested plant
299 tissues, while *SUT1* only provided resistance in hydathodes (Figure 5G).

300

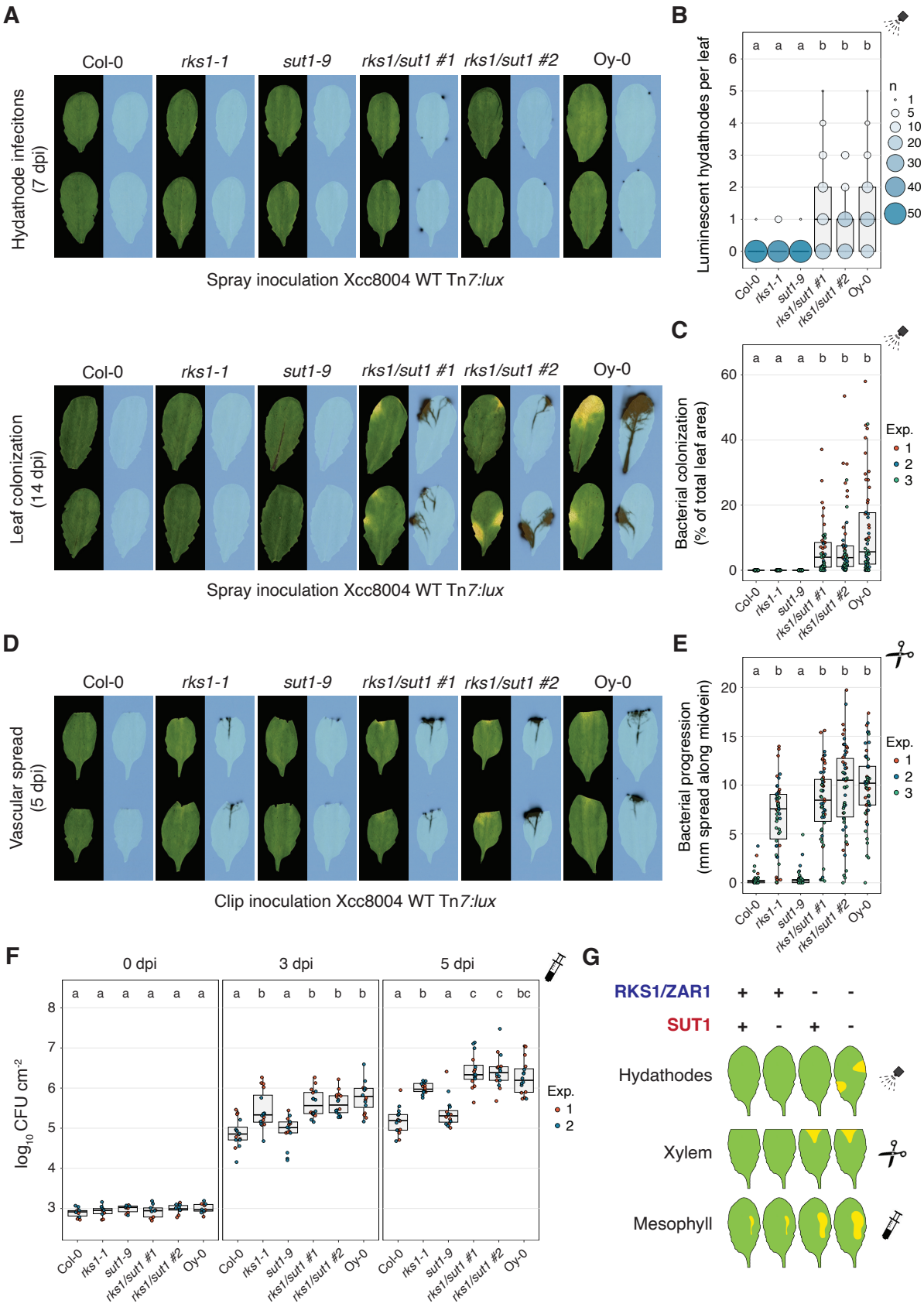
A
Col-0
rks1-1
sut1-9
rks1/sut1 #1
rks1/sut1 #2
Oy-0
Hydathode infecitons (7 dpi)
Spray inoculation Xcc8004 WT Tn7:lux
B
Luminescent hydathodes per leaf
n
1
5
10
20
30
40
50
C
Leaf colonization (14 dpi)
Bacterial colonization (% of total leaf area)
Exp.
1
2
3
D
Vascular spread (5 dpi)
Clip inoculation Xcc8004 WT Tn7:lux
E
Bacterial progression (mm spread along midvein)
F
0 dpi
3 dpi
5 dpi
log10 CFU cm-2
G
RKS1/ZAR1
SUT1
Hydathodes
Xylem
Mesophyll

301

302

303 **Figure 5. *RKS1/ZAR1* and *SUT1* confer resistance to Xcc in different stages of infection. A)** Spray inoculation with
304 Xcc8004 Tn*7:lux* on *rks1-1* and *sut1-9* single mutants and two independent *rks1/sut1* CRISPR knockout lines with
305 wildtype background Col-0 and accession Oy-0 as controls. *Top,* visualization of Xcc hydathode colonization using light
306 sensitive films (7 dpi); *bottom*, visualization of the systemic spread of Xcc and disease symptom development (14 dpi).
307 **B,C)** Quantification of panel A as number of infected hydathodes per leaf at 7 dpi (**B**) and bacterial colonization (**C**) at
308 14 dpi (n = 18 leaves per experiment). **D)** Clip inoculation with Xcc8004 Tn*7:lux* on the same plant lines used in panel
309 A. **E)** Quantification of bacterial progression along the midvein of panel D at 5 dpi (n = 18 leaves per experiment). **F)**
310 Colony forming units at 0, 3 and 5 days post syringe inoculation of Xcc8004 WT Tn*7:lux* in the apoplast of the plant lines
311 used in panel A (n = 8 samples per experiment. **G)** Schematic model indicating the contribution to resistance by
312 *RKS1/ZAR1* and *SUT1* in different leaf tissues.

313 **Discussion**

314 Here, we characterized a role for Arabidopsis SUT1 as a functional immune receptor in natural
315 infections by Xcc. We showed that SUT1 acts in hydathodes, restricting Xcc colonization in the
316 initial stage of the infection and thereby reducing the subsequent systemic spread of Xcc and
317 with that the onset of disease symptoms. Interestingly, SUT1 resistance was strongly
318 compromised when the hydathodes were bypassed, indicating that SUT1 confers a first layer of
319 defense in the Xcc disease cycle. We found that this role of SUT1 contrasts sharply with the
320 previously characterized RKS1/ZAR1 immune response triggered by XopAC [24,25]. The
321 resistance conferred by this so-called ZAR1-resistosome in different plant tissues can be
322 explained by its role in broad-spectrum resistance against the mesophyll pathogen Pst [41] and
323 the vascular Xcc. So far, no evidence exists for a role of SUT1 in immunity against mesophyll
324 pathogens [31], which might explain why it only confers resistance to Xcc in hydathodes. Yet, our
325 data indicates expression of *SUT1* in hydathodes as well as the mesophyll, which is corroborated
326 by several recent single-cell transcriptomics studies [13,37,38]. Nonetheless, the resistance
327 conferred by SUT1 in the mesophyll against Xcc remains limited compared to the complete
328 resistance found in hydathodes (Figure 5), suggesting that the expression of a putative guardee or
329 bacterial elicitor could be tissue-specific. Indications for this can be found in recent work on the

330 HrpG virulence regulon of 17 *Xanthomonas* spp., which revealed that not all virulence factors are
331 controlled by HrpG, highlighting the possibility of temporal regulation of secreted virulence
332 factors by *Xanthomonas* during infection [42]. In addition, the absence of vascular immunity
333 conferred by SUT1 remains atypical, as different vascular immune responses against Xcc have
334 been identified, such as XOPAM ACTIVATED RESISTANCE 1(AMAR1)-mediated hypersensitive
335 response through interaction with the T3E XopAM [43] and MAPK signaling cascades that lead to
336 reduced vascular spread and symptom development when Xcc is directly introduced into the
337 vasculature [23]. Therefore, the role of SUT1 in plant defense seems optimized for hydathodes
338 and this role is unique compared to any other studied Arabidopsis NLRs to date [17,44].

339 As *SUT1* encodes an intracellular immune receptor, our data support the notion that Xcc actively
340 manipulates the epithem tissue to gain access to the plant vasculature. Importantly, the causal
341 agent for SUT1 immune activation remains unknown albeit that an indirect activation mechanism
342 has been proposed where SUT1 guards the TOPP4 phosphatase has been proposed in the context
343 of autoimmunity [31]. While we did not find evidence for this TOPP4 guard-guardee model in the
344 interaction with Xcc (Figure S3), the two closest homologs of SUT1 in Arabidopsis, RESISTANT TO
345 P. SYRINGAE 5 (RPS5) and SUPPRESSOR OF MKK1 MKK2 2 (SUMM2) [31], have both been
346 described as 'guards' in plant-pathogen interactions [45,46], which argues in favor of the
347 possibility of a similar guard function of SUT1. In addition, AlphaFold3 has very recently been
348 leveraged to distinguish between helper and sensor functions of plant NLRs, which could also be
349 used to predict the function of SUT1 in pathogen recognition [47].

350 Indications for the immune elicitor could be found in the putative guardee TOPP4, which is part
351 of an Arabidopsis gene family of highly similar protein phosphatases called TOPP1 to TOPP9. This
352 family is involved in abscisic acid (ABA) signaling and leaf water homeostasis [48,49].
353 Interestingly, multiple TOPP family members are targeted by the *Pseudomonas syringae* T3E AvrE
354 during infection to hijack ABA signaling, thereby suppressing the re-opening of the stomata upon

355 bacterial entry to induce water soaking of the leaf apoplast—a phenomenon that supports
356 bacterial colonization of the leaf apoplast [50–52]. Notably, Xcc8004 is known to employ the T3E
357 XopAM, which belongs to the same protein superfamily of conserved bacterial effectors as
358 *Pseudomonas* AvrE [53]. Nonetheless, the AvrE superfamily members can exhibit a wide variety
359 of functions [54] and recent work using a yeast two-hybrid screen on an Arabidopsis cDNA library
360 did not reveal a protein-protein interaction between XopAM and individual TOPPs [43]. Although
361 the elicitor of SUT1-mediated resistance has not been identified, it might be associated with
362 manipulation of TOPPs and therefore ABA signaling.

363 When it comes to hydathode colonization, we see an intermediate level of resistance in the *sut1*
364 knockout lines in the Col-0 background compared to the susceptible accession Oy-0. This
365 indicates the presence of additional resistance mechanisms in Col-0 against Xcc in hydathodes.
366 Indeed, we observed two additional minor QTLs on Chromosome 4, which were not further fine
367 mapped in this study. The underlying genes for these QTLs might encode additional NLRs,
368 receptor-like proteins (RLPs), receptor-like kinases (RLKs) or guardees of SUT1, some of which
369 are even known to be specifically expressed in hydathodes [55]. It seems that the resistance
370 phenotype seen in Col-0, in absence of RKS1/ZAR1-mediated resistance, can still be based on
371 several and possibly disconnected resistance mechanisms of which SUT1 resistance appears to
372 be a major contributor. The existence of a wide array of immune receptors in Arabidopsis holds
373 promise for application of these genes in *Brassica* crops to ensure durable resistance using a
374 transgene approach. As was shown in other crop-pathogen interactions, *R* gene stacking is less
375 readily overcome by pathogens than the implementation of single *R* genes [56–58].

376 The identification of *SUT1* was made possible through the RIL analysis, as the GWA analysis itself
377 did not lead to significantly correlating SNPs in *SUT1*. In these analyses, assessing disease
378 severity relied on luminescence index scoring at 14 dpi [27], which could have reduced the
379 likelihood of identifying resistance mechanisms in the early stages of infection in these large

380 natural populations. For this reason, our lab has put efforts into the development of quantitative
381 image analysis methods for bacterial bioluminescence [59]. In addition, we have developed a
382 non-invasive imaging method to track bacterial infections in Arabidopsis rosettes over time, from
383 hydathodes to mesophyll [60]. Work is in progress to repeat the GWA study using the improved
384 temporal resolution offered by this non-invasive imaging setup, thus increasing the likelihood of
385 identifying additional genetic factors in Arabidopsis that play a role in hydathode resistance
386 against Xcc.

387 In summary, we identified a CNL-type immune receptor, SUT1, that acts in hydathodes where it
388 reduces Xcc virulence by limiting the initial hydathode colonization and thereby the subsequent
389 disease progression. This SUT1 resistance against Xcc seems to be limited to hydathodes, as the
390 efficacy of the *SUT1* gene was lost when the initial hydathode barrier was breached. Future
391 studies should aim to solve how SUT1 immunity is activated by Xcc, although SUT1 likely acts as
392 a guard of one or more TOPPs or other plant phosphatases.

Materials and Methods

Plant growth conditions

Arabidopsis thaliana lines used are listed in S1 Table. For all experiments, seeds were stratified for three to four days on wet filter paper at 4 °C in the dark, and then sown in 40-pot trays (Desh Plantpak, Tray Danish size 40 cell (8x5)) in slitpots (Pöppelmann Teku, S 5,5 LB), using potting soil (Jongkind Substrates, Hol80 zaaigrond Nr 1) to which 500 ml Entonem suspension (Koppert Biological Systems, approximately 1.6 x 10^6 third stage *Steinernema feltiae* nematode larvae) was added per tray to prevent black fly multiplication in growth chambers. Hereafter, trays were placed in standard short day (SD) conditions (11/13h light/dark, 22 °C, RH 70%). For the first five days after sowing, trays were covered with transparent plastic domes to ensure seedling growth.

Generation of Arabidopsis reporter lines

Primer sequences and plasmids used are listed in S1 Table. The plasmids to create the *pSUT1::GUS* and *pSUT1::NLS-3×mVENUS* reporter lines in Arabidopsis were assembled using the GreenGate system [61]. First, a 2.1 kb fragment upstream of the start codon of *SUT1* (*AT5G63020*) in Col-0, which also covers the 119 bp 5'UTR indicated by RNA-seq data [32], was synthesized with external *Bsa*I sites (Eurofins Genomics). As the entire adjacent gene (AT5G63030) falls within this region, four potential start codons were modified. Next, the *NLS-3×mVENUS* module was amplified from pGreenII-229-NLS-3×mVENUS [36] with added *Bsa*I sites and cloned into pGGA000. Final binary vectors were then assembled in the backbone pGGZ003 with either *GUS* or *NLS-3×mVENUS* as CDS module using a multisite Goldengate reaction, leading to pGGZ_pSUT1_GUS_tUBQ10_BastaR and pGGZ_SUT1_NLS-3×mVENUS_tUBQ10_BastaR. These plasmids were electroporated into *Agrobacterium tumefaciens* strain GV3101 carrying pSOUP and Arabidopsis Col-0 was transformed using the floral dip method [62]. Two independent GUS lines and three independent *NLS-3×mVENUS* lines were used for imaging.

417 **Generation of Arabidopsis Col-0 *rks1/sut1* knockout lines using CRISPR/zCas9i**

418 Primer sequences and plasmids used are listed in S1 Table. The constructs to generate *rks1/sut1*
419 double knockouts were assembled using the zCas9i cloning kit from Addgene (#1000000171).
420 First, for each target gene, two individual guide sequences were designed on the Col-0 alleles
421 using the webtool CRISPR P (v2.0). Next, these four individual guides were cloned into their
422 respective pDGE shuttle vectors using BpiI, followed by assembly in the multiplex destination
423 vector pDGE652 using BsaI. The resulting plasmid was then electroporated into *Agrobacterium*
424 *tumefaciens* GV3101 and Arabidopsis Col-0 was transformed using the floral dip method [62]. T1
425 seeds were selected through the *pOLE1:OLE1-RFP* seed coat marker using the Rhodamine filter
426 in Bio-Rad ChemiDoc imager. Next, DNA was extracted from T1 plants using the ThermoFisher
427 Kingfisher Apex and MagMAX Plant DNA Isolation Kit according to manufacturer's instructions.
428 Guide target regions were PCR amplified with Phusion DNA Polymerase using flanking primers
429 and sent for Sanger sequencing and subsequent Synthego ICE analysis. Two individual
430 transformants were selected that exhibited confirmed biallelic knockouts (through early stop
431 codons) in both *RKS1* and *SUT1* (Figure S7) and were propagated into the next generation. The
432 resulting T2 plants were used for Xcc disease assays (Figure 5).

433 **Generation of bioluminescent Xcc strain**

434 All bacterial strains, plasmids and oligonucleotides used are listed in S1 Table. Wildtype Xcc8004
435 was tagged with a double bioluminescence/fluorescence cassette using the mini-Tn7 transposon
436 system [63,64]. Recipient strain Xcc8004 was co-incubated on LB plates with one donor *E. coli*
437 strain (DH5α + pRS-Tn7-*pNPTII*::*lux-pA1*::*mTq2* [16,64]) and two helper *E. coli* strains; one carrying
438 Tn7 transposon genes *tnsABCDE* (DH5α + pUX-BF13 [65]) and one carrying a plasmid that
439 facilitates conjugation (HB101 + pRK2073 [66]). Next, cultures were collected and transformants
440 were selected on LB plates with antibiotics (20 µg/ml nitrofurantoin and 50 µg/ml kanamycin) and
441 checked for luminescence using the ChemiDoc MP imager (Bio-Rad).

442 ***Xanthomonas* disease assays**

443 Spray inoculations with bioluminescent Xcc8004 WT or *ΔxopAC* (Tn*5:lux* or Tn*7:lux*) strain were
444 performed according to previous studies [27,16]. Briefly, Xcc strains were plated on KADO
445 medium [67] with the appropriate antibiotics and grown for 48-72 hours at 28 °C. Bacteria were
446 collected, washed once with 10 mM $MgSO_4$ and diluted to OD_{600} = 0.1. Silwet L-77 was added to
447 a final concentration of 0.0002% and bacteria were sprayed on 4-to-5-week-old Arabidopsis
448 plants (Preval sprayer, SKU# 0221). Inoculated plants were subjected to two guttation cycles over
449 two days in a climate incubator (Snijders Labs, MC1000) to promote hydathode infection. In these
450 cycles, temperature and relative humidity were raised (25°C, RH 95%) to induce guttation, after
451 which a rapid drop in temperature and humidity (21°C, RH 70%) leads to re-uptake of guttation
452 droplets. Subsequently, plants were placed for an additional 12 days at SD growth conditions
453 (11/13h light/dark, 24-22 °C, RH 70%) in the same incubator. Clipping assays were performed by
454 cutting 5 mm of the apex of each leaf (three leaves per plant) with scissors dipped in bacterial
455 inoculum (OD_{600} = 0.1). Plants were subjected to the same two-day guttation cycle and placed for
456 an additional five days at SD growth conditions in an MC1000 climate chamber.

457 Syringe inoculations were performed by infiltrating bacterial inoculum (OD_{600} = 0.0001) into the
458 apoplast of each leaf (three leaves per plant) with a needleless 1 ml syringe. Plants were covered
459 with a plastic dome to ensure high humidity conditions and grown for an additional five days at
460 SD growth conditions. To determine CFU counts after leaf infiltration, at 0, 3 and 5 dpi, two leaf
461 discs (5 mm diameter) were taken from each infiltrated leaf with a leaf puncher, placed into 500
462 µl 10 mM $MgSO_4$ containing two steel beads and homogenized twice for 1 minute at 30 Hz in a
463 TissueLyser II (QIAGEN). Samples were serially diluted and plated on KADO agar plates
464 containing 50 µg/ml kanamycin. After 24h, colonies were counted and log CFU per cm^2 leaf
465 material (log_{10} CFU cm^{-2}) was calculated.

466 **Detection of luminescent bacteria**

467 For spray inoculations, the three most diseased leaves of each plant were sampled 7 dpi and 14
468 dpi. Each leaf was glued onto an A3 white paper sheet using a grid and covered with a transparent
469 plastic sheet [27]. Next, a light-sensitive X-ray film (Fuji Super RX) was placed on top and left for
470 exposure overnight. The film was developed the next morning and scanned, alongside the leaves,
471 using an A3 flatbed scanner (Epson Expression 12000XL). For 7 dpi, the obtained images were
472 overlayed in Adobe Photoshop 2023/2024 to count the number of luminescent hydathodes per
473 leaf. At 14 dpi, scans of leaves and light-sensitive film were analyzed using the ScAnalyzer image
474 analysis script [59] to determine chlorosis and bacterial colonization. For clipping assays, at 7
475 dpi, leaves were sampled in the same manner. For analysis, chlorosis and bacterial colonization
476 were analyzed with ScAnalyzer. Bacterial progression through the midvein was measured using
477 Fiji (ImageJ).

478 **RIL screen and QTL analysis**

479 The Oy-0 × Col-0 RIL population [26] was received from the INRAE/IJPB Versailles stock center.
480 From the 470 RILs in the population, 165 (including the parental Oy-0 and Col-0) were selected
481 for disease assays (Extended Data 1). For analysis, the mean luminescence index score [27] per
482 leaf (n = 18) for each line was normalized to the score of Oy-0 and used as input for QTL mapping
483 in R using the R/qtl package version 1.66 [28]. LOD scores for each of the 85 markers were
484 determined in a single QTL model using the Expectation-maximization (EM) algorithm. LOD
485 thresholds were determined by permutation (n = 1000). Explained variance (EV) per QTL was
486 calculated as $EV(\%) = (1 - 10(-2 * LOD/n) * 100$, where LOD is the LOD score and n is the
487 number of RILs.

488 **GWA screen and analysis**

489 The HapMap seed collection was received from NASC and propagated (Borevitz lab; NASC ID,
490 N76309; ABRC ID, CS76309). From the 360 lines in the population, 321 accessions (including the
491 controls Oy-0 and Col-0) could be propagated for disease assays (Extended Data 2). The mean
492 luminescence index score [27] per leaf (n = 18) for each line was normalized to Oy-0. As input for
493 GWA analysis, the data was transformed in a binary score in which 0 = <50% and 1 = >50% of Oy-
494 0. These phenotypes were analyzed in the GWA portal [30] using the Imputed Full sequence
495 Dataset, TAIR 9, containing over five million SNPs [68]. P-values were obtained by applying an
496 accelerated mixed model (AMM) [69]. False Discovery Rate (FDR) thresholds were set at $-\log_{10}(p)$
497 = 8 (Bonferroni) and $-\log_{10}(p)$ = 7.29 (Benjamini-Hochberg). All SNPs with $-\log_{10}(p)$ values >6 are
498 listed in Extended Data 2.

499 **GUS staining and imaging**

500 Transgenic GUS lines were grown for 4-5 weeks at standard SD conditions. Rosettes were taken
501 from soil, washed in double distilled water and submerged in GUS staining solution (0.5 mM
502 $K_3Fe(CN)_6$, 0.5 mM $K_4Fe(CN)_6$, 0.1 M $NaPO_4$ (pH 7.0), 10 mM EDTA, 0.1% (v/v) Triton X-100 and 1
503 mg/ml X-Gluc in double distilled water) [70] in a 50 ml falcon tube. Rosettes were vacuum
504 infiltrated twice for two minutes and then incubated at 37 °C for two hours to avoid overstaining
505 [70]. To destain, rosettes were incubated in 96% ethanol at room temperature for two days. The
506 destaining solution was replaced twice until all chlorophyll had been removed. Leaves were
507 imaged using a stereomicroscope (Leica MZ FLIII + Nikon Digital Sight DS-Fi2).

508 **Imaging fluorescent reporter lines**

509 Fluorescent reporter lines were grown for 4-5 weeks using SD conditions (13D/11L). To enable
510 imaging of exposed hydathode tissue, fully expanded leaves were picked and stripped of the
511 epidermal cell layer [71] using household sellotape. Leaves were then imaged with a digital

512 inverted fluorescence microscope (ThermoFisher EVOS fl, RFP filter for tdTomato, YFP filter for
513 mVENUS).

514 **Protein sequence alignments**

515 Col-0 and Oy-0 whole genome assemblies and annotations [32] were downloaded from NCBI.
516 Coding sequences from both *SUT1*$^{Col-0}$ and *SUT1*$^{Oy-0}$ were extracted and translated *in silico*.
517 Predicted protein sequences were then aligned in R with ClustalOmega using the Biostrings
518 (v.2.68.1) and msa (v.1.32.0) packages.

519 **Quantification and statistical analyses**

520 All data analyses and plotting were done in R (v.4.3.2). All experiments were performed as
521 independent repetitions shown in each figure. Number of biological replicates is mentioned in
522 each figure legend. Data from repetitions was pooled for visualization and statistical analysis.

523 **Acknowledgements**

524 We would like to thank Ludek Tikovsky and Harold Lemereis for the excellent care of our plants in
525 the greenhouse. We also want to thank Manon Richard for previous work on fluorescent reporter
526 lines in Arabidopsis. Lastly, we want to thank Niko Geldner, Laurent Noël and Gail Preston for
527 sharing materials. This research was supported by the Topsector T&U TKI programs "Stop natural
528 entry" and "Finding the Achilles' heel of Brassica for Black Rot disease" (grants EZ-2012-02 and
529 TU18024 to H.A.v.d.B.), an NWO-XS grant (OCENW.XS24.1.155 to S.P.) and the breeding
530 companies Bejo Zaden B.V. and Rijk Zwaan.

531 **Competing interests**

532 H.A.v.d.B. is currently an employee of Rijk Zwaan. This work was supported in part by a grant from
533 Rijk Zwaan and Bejo Zaden. Both companies had no role in the design of the study, data
534 collection, and writing of the manuscript.

References

1. Melotto M, Zhang L, Oblessuc PR, He SY. Stomatal Defense a Decade Later. Plant Physiol. 2017 Jun;174(2):561–71. https://doi.org/10.1104/pp.16.01853

2. Zhang J, Coaker G, Zhou JM, Dong X. Plant Immune Mechanisms: From Reductionistic to Holistic Points of View. Mol Plant. 2020 Oct;13(10):1358–78. https://doi.org/10.1016/j.molp.2020.09.007

3. Zipfel C, Robatzek S, Navarro L, Oakeley EJ, Jones JDG, Felix G, et al. Bacterial disease resistance in *Arabidopsis* through flagellin perception. Nature. 2004 Apr 1;428(6984):764–7. https://doi.org/10.1038/nature02485

4. Miya A, Albert P, Shinya T, Desaki Y, Ichimura K, Shirasu K, et al. CERK1, a LysM receptor kinase, is essential for chitin elicitor signaling in *Arabidopsis*. Proc Natl Acad Sci. 2007;104(49):19613–8. https://doi.org/10.1073/pnas.0705147104

5. Liu Z, Hou S, Rodrigues O, Wang P, Luo D, Munemasa S, et al. Phytocytokine signalling reopens stomata in plant immunity and water loss. Nature. 2022 May 12;605(7909):332–9. https://doi.org/10.1038/s41586-022-04684-3

6. Melotto M, Underwood W, Koczan J, Nomura K, He SY. Plant Stomata Function in Innate Immunity against Bacterial Invasion. Cell. 2006 Sep;126(5):969–80. https://doi.org/10.1016/j.cell.2006.06.054

7. Thor K, Jiang S, Michard E, George J, Scherzer S, Huang S, et al. The calcium-permeable channel OSCA1. 3 regulates plant stomatal immunity. Nature. 2020;585(7826):569–73. https://doi.org/10.1038/s41586-020-2702-1

8. Cerutti A, Jauneau A, Auriac MC, Lauber E, Martinez Y, Chiarenza S, et al. Immunity at Cauliflower Hydathodes Controls Systemic Infection by *Xanthomonas campestris* pv *campestris*. Plant Physiol. 2017 Jun;174(2):700–16. https://doi.org/10.1104/pp.16.01852

9. Gluck-Thaler E, Cerutti A, Perez-Quintero AL, Butchacas J, Roman-Reyna V, Madhavan VN, et al. Repeated gain and loss of a single gene modulates the evolution of vascular plant pathogen lifestyles. Sci Adv. 2020 Nov 13;6(46):eabc4516. https://doi.org/10.1126/sciadv.abc4516

10. Hugouvieux V, Barber CE, Daniels MJ. Entry of *Xanthomonas campestris* pv. *campestris* into Hydathodes of *Arabidopsis thaliana* Leaves: A System for Studying Early Infection Events in Bacterial Pathogenesis. Mol Plant-Microbe Interactions®. 1998 Jun;11(6):537–43. https://doi.org/10.1094/MPMI.1998.11.6.537

11. Cerutti A, Jauneau A, Laufs P, Leonhardt N, Schattat MH, Berthomé R, et al. Mangroves in the Leaves: Anatomy, Physiology, and Immunity of Epithemal Hydathodes. Annu Rev Phytopathol. 2019 Aug 25;57(1):91–116. https://doi.org/10.1146/annurev-phyto-082718-100228

12. Jauneau A, Cerutti A, Auriac MC, Noël LD. Anatomy of leaf apical hydathodes in four monocotyledon plants of economic and academic relevance. PLoS One. 2020;15(9):e0232566. https://doi.org/10.1371/journal.pone.0232566

13. Routaboul J, Bellenot C, Olympio A, Clément G, Citerne S, Remblière C, et al. *Arabidopsis* hydathodes are sites of auxin accumulation and nutrient scavenging. Plant J. 2024 Nov;120(3):857–71. https://doi.org/10.1111/tpj.17014

14. Bellenot C, Routaboul JM, Laufs P, Noël LD. Hydathodes. Curr Biol. 2022;32(14):R763–4. https://doi.org/10.1016/j.cub.2022.06.014

15. Jian Y, Gong D, Wang Z, Liu L, He J, Han X, et al. How plants manage pathogen infection. EMBO Rep. 2024;25(1):31–44. https://doi.org/10.1038/s44319-023-00023-3

16. Paauw M, van Hulten M, Chatterjee S, Berg JA, Taks NW, Giesbers M, et al. Hydathode immunity protects the *Arabidopsis* leaf vasculature against colonization by bacterial pathogens. Curr Biol. 2023 Feb;S0960982223000131. https://doi.org/10.1016/j.cub.2023.01.013

17. Ngou BPM, Ding P, Jones JDG. Thirty years of resistance: Zig-zag through the plant immune system. Plant Cell. 2022 May 1;34(5):1447–78. https://doi.org/10.1093/plcell/koac041

18. Ngou BPM, Jones JDG, Ding P. Plant immune networks. Trends Plant Sci. 2022 Mar;27(3):255–73. https://doi.org/10.1016/j.tplants.2021.08.012

19. Büttner D. Behind the lines–actions of bacterial type III effector proteins in plant cells. FEMS Microbiol Rev. 2016;40(6):894–937. https://doi.org/10.1093/femsre/fuw026

20. Contreras MP, Lüdke D, Pai H, Toghani A, Kamoun S. NLR receptors in plant immunity: making sense of the alphabet soup. EMBO Rep. 2023 Oct 9;24(10):e57495. https://doi.org/10.15252/embr.202357495

21. Wang J, Hu M, Wang J, Qi J, Han Z, Wang G, et al. Reconstitution and structure of a plant NLR resistosome conferring immunity. Science. 2019;364(6435):eaav5870. https://dx.doi.org/10.1126/science.aav5870

22. Xin XF, Kvitko B, He SY. Pseudomonas syringae: what it takes to be a pathogen. Nat Rev Microbiol. 2018 May;16(5):316–28. https://doi.org/10.1038/nrmicro.2018.17

23. Lin H, Wang M, Chen Y, Nomura K, Hui S, Gui J, et al. An MKP-MAPK protein phosphorylation cascade controls vascular immunity in plants. Sci Adv. 2022;8(10):eabg8723. https://doi.org/10.1126/sciadv.abg8723

24. Wang G, Roux B, Feng F, Guy E, Li L, Li N, et al. The decoy substrate of a pathogen effector and a pseudokinase specify pathogen-induced modified-self recognition and immunity in plants. Cell Host Microbe. 2015;18(3):285–95. http://dx.doi.org/10.1016/j.chom.2015.08.004

25. Guy E, Lautier M, Chabannes M, Roux B, Lauber E, Arlat M, et al. xopAC-triggered Immunity against *Xanthomonas* Depends on *Arabidopsis* Receptor-Like Cytoplasmic Kinase Genes PBL2 and RIPK. Yang CH, editor. PLoS ONE. 2013 Aug 9;8(8):e73469. https://doi.org/10.1371/journal.pone.0073469

26. Simon M, Loudet O, Durand S, Bérard A, Brunel D, Sennesal FX, et al. QTL mapping in five new large RIL populations of *Arabidopsis thaliana* genotyped with consensus SNP markers. Genetics. 2008;178(2253):64. https://doi.org/10.1534/genetics.107.083899

27. van Hulten M, Chatterjee S, van den Burg HA. Infection Assay for *Xanthomonas campestris* pv. *campestris* in *Arabidopsis thaliana* Mimicking Natural Entry via Hydathodes. In: Plant Innate Immunity. Humana, New York, NY: Springer; 2019. p. 159–85. Available from: https://doi.org/10.1007/978-1-4939-9458-8_16

28. Broman KW, Wu H, Sen Ś, Churchill GA. R/qtl: QTL mapping in experimental crosses. bioinformatics. 2003;19(7):889–90. https://doi.org/10.1093/bioinformatics/btg112

29. Weigel D, Mott R. The 1001 genomes project for *Arabidopsis thaliana*. Genome Biol. 2009;10:1–5. https://doi.org/10.1186/gb-2009-10-5-107

30. Seren Ü. GWA-Portal: Genome-Wide Association Studies Made Easy. In: Ristova D, Barbez E, editors. Root Development: Methods and Protocols. New York, NY: Springer New York; 2018. p. 303–19. https://doi.org/10.1007/978-1-4939-7747-5_22

31. Yan J, Liu Y, Huang X, Li L, Hu Z, Zhang J, et al. An unreported NB-LRR protein SUT1 is required for the autoimmune response mediated by type one protein phosphatase 4 mutation (topp4-1) in Arabidopsis. Plant J. 2019;100(2):357–73. https://doi.org/10.1111/tpj.14447

32. Lian Q, Huettel B, Walkemeier B, Mayjonade B, Lopez-Roques C, Gil L, et al. A pan-genome of 69 *Arabidopsis thaliana* accessions reveals a conserved genome structure throughout the global species range. Nat Genet. 2024 May;56(5):982–91. https://doi.org/10.1038/s41588-024-01715-9

33. Padmanabhan M, Cournoyer P, Dinesh-Kumar SP. The leucine-rich repeat domain in plant innate immunity: a wealth of possibilities. Cell Microbiol. 2009;11(2):191–8. https://doi.org/10.1111/j.1462-5822.2008.01260.x

34. Martin R, Qi T, Zhang H, Liu F, King M, Toth C, et al. Structure of the activated ROQ1 resistosome directly recognizing the pathogen effector XopQ. Science. 2020;370(6521):eabd9993. https://doi.org/10.1126/science.abd9993

35. Hull GA, Devic M. The β-Glucuronidase (gus) Reporter Gene System. In: Jones H, editor. Plant Gene Transfer and Expression Protocols. Totowa, NJ: Springer New York; 1995. p. 125–41. https://doi.org/10.1385/0-89603-321-X:125

36. Zhou F, Emonet A, Dénervaud Tendon V, Marhavy P, Wu D, Lahaye T, et al. Co-incidence of Damage and Microbial Patterns Controls Localized Immune Responses in Roots. Cell. 2020 Feb;180(3):440-453.e18. https://doi.org/10.1016/j.cell.2020.01.013

37. Tang B, Feng L, Hulin MT, Ding P, Ma W. Cell-type-specific responses to fungal infection in plants revealed by single-cell transcriptomics. Cell Host Microbe. 2023 Oct;31(10):1732-1747.e5. https://doi.org/10.1016/j.chom.2023.08.019

38. Kim JY, Symeonidi E, Pang TY, Denyer T, Weidauer D, Bezrutczyk M, et al. Distinct identities of leaf phloem cells revealed by single cell transcriptomics. Plant Cell. 2021 May 5;33(3):511–30. https://doi.org/10.1093/plcell/koaa060

39. Huard-Chauveau C, Perchepied L, Debieu M, Rivas S, Kroj T, Kars I, et al. An Atypical Kinase under Balancing Selection Confers Broad-Spectrum Disease Resistance in *Arabidopsis*. McDowell JM, editor. PLoS Genet. 2013 Sep 12;9(9):e1003766. https://doi.org/10.1371/journal.pgen.1003766

40. Stuttmann J, Barthel K, Martin P, Ordon J, Erickson JL, Herr R, et al. Highly efficient multiplex editing: one-shot generation of 8× *Nicotiana benthamiana* and 12× Arabidopsis mutants. Plant J. 2021 Apr;106(1):8–22. https://doi.org/10.1111/tpj.15197

41. Lewis JD, Lee AHY, Hassan JA, Wan J, Hurley B, Jhingree JR, et al. The *Arabidopsis* ZED1 pseudokinase is required for ZAR1-mediated immunity induced by the *Pseudomonas syringae* type III effector HopZ1a. Proc Natl Acad Sci. 2013 Nov 12;110(46):18722–7. https://doi.org/10.1073/pnas.1315520110

42. Monnens TQ, Roux B, Cunnac S, Charbit E, Carrère S, Lauber E, et al. Comparative transcriptomics reveals a highly polymorphic *Xanthomonas* HrpG virulence regulon. BMC Genomics. 2024 Aug 9;25(1):777. https://doi.org/10.1186/s12864-024-10684-6

43. Xie Q, Wei B, Zhan Z, He Q, Wu K, Chen Y, et al. Arabidopsis membrane protein AMAR1 interaction with type III effector XopAM triggers a hypersensitive response. Plant Physiol. 2023 Dec 1;193(4):2768–87. https://doi.org/10.1093/plphys/kiad478

44. Van de Weyer AL, Monteiro F, Furzer OJ, Nishimura MT, Cevik V, Witek K, et al. A species-wide inventory of NLR genes and alleles in *Arabidopsis thaliana*. Cell. 2019;178(5):1260-1272. e14. https://doi.org/10.1016/j.cell.2019.07.038

45. Pottinger SE, Innes RW. RPS5-mediated disease resistance: fundamental insights and translational applications. Annu Rev Phytopathol. 2020;58:139–60. https://doi.org/10.1146/annurev-phyto-010820-012733

46. Zhang Z, Wu Y, Gao M, Zhang J, Kong Q, Liu Y, et al. Disruption of PAMP-induced MAP kinase cascade by a *Pseudomonas syringae* effector activates plant immunity mediated by the NB-LRR protein SUMM2. Cell Host Microbe. 2012;11(3):253–63. https://doi.org/10.1016/j.chom.2012.01.015

47. Toghani A, Frijters R, Bozkurt TO, Terauchi R, Kamoun S, Sugihara Y. Can AI modelling of protein structures distinguish between sensor and helper NLR immune receptors? bioRxiv; 2024 [cited 2024 Dec 5]. https://doi.org/10.1101/2024.11.24.625045

48. Hou YJ, Zhu Y, Wang P, Zhao Y, Xie S, Batelli G, et al. Type one protein phosphatase 1 and its regulatory protein inhibitor 2 negatively regulate ABA signaling. PLoS Genet. 2016;12(3):e1005835. https://doi.org/10.1371/journal.pgen.1005835

49. Zhang J, Qin Q, Nan X, Guo Z, Liu Y, Jadoon S, et al. Role of protein phosphatase1 regulatory subunit3 in mediating the abscisic acid response. Plant Physiol. 2020;184(3):1317–32. https://doi.org/10.1104/pp.20.01018

50. Hu Y, Ding Y, Cai B, Qin X, Wu J, Yuan M, et al. Bacterial effectors manipulate plant abscisic acid signaling for creation of an aqueous apoplast. Cell Host Microbe. 2022;30(4):518-529. e6. https://doi.org/10.1016/j.chom.2022.02.002

51. Roussin-Léveillée C, Lajeunesse G, St-Amand M, Veerapen VP, Silva-Martins G, Nomura K, et al. Evolutionarily conserved bacterial effectors hijack abscisic acid signaling to induce an aqueous environment in the apoplast. Cell Host Microbe. 2022 Apr;30(4):489-501.e4. https://doi.org/10.1016/j.chom.2022.02.006

52. Xin XF, Nomura K, Aung K, Velásquez AC, Yao J, Boutrot F, et al. Bacteria establish an aqueous living space in plants crucial for virulence. Nature. 2016 Nov;539(7630):524–9. https://doi.org/10.1038/nature20166

53. Degrave A, Siamer S, Boureau T, Barny MA. The AvrE superfamily: ancestral type III effectors involved in suppression of pathogen-associated molecular pattern-triggered immunity: The AvrE superfamily of type III effectors. Mol Plant Pathol. 2015 Oct;16(8):899–905. https://doi.org/10.1111/mpp.12237

54. Nomura K, Andreazza F, Cheng J, Dong K, Zhou P, He SY. Bacterial pathogens deliver water-and solute-permeable channels to plant cells. Nature. 2023;621(7979):586–91. https://doi.org/10.1038/s41586-023-06531-5

55. Wu Y, Xun Q, Guo Y, Zhang J, Cheng K, Shi T, et al. Genome-wide expression pattern analyses of the *Arabidopsis* leucine-rich repeat receptor-like kinases. Mol Plant. 2016;9(2):289–300. http://dx.doi.org/10.1016/j.molp.2015.12.011

56. Shehryar K, Khan RS, Iqbal A, Hussain SA, Imdad S, Bibi A, et al. Transgene stacking as effective tool for enhanced disease resistance in plants. Mol Biotechnol. 2020;62:1–7. https://doi.org/10.1007/s12033-019-00213-2

57. Zhang J, Hewitt TC, Boshoff WH, Dundas I, Upadhyaya N, Li J, et al. A recombined Sr26 and Sr61 disease resistance gene stack in wheat encodes unrelated NLR genes. Nat Commun. 2021;12(1):3378. https://doi.org/10.1038/s41467-021-23738-0

58. Zhu S, Li Y, Vossen JH, Visser RG, Jacobsen E. Functional stacking of three resistance genes against *Phytophthora infestans* in potato. Transgenic Res. 2012;21:89–99. https://doi.org/10.1007/s11248-011-9510-1

59. Paauw M, Hardeman G, Taks NW, Lambalk L, Berg JA, Pfeilmeier S, et al. ScAnalyzer: an image processing tool to monitor plant disease symptoms and pathogen spread in *Arabidopsis thaliana* leaves. Plant Methods. 2024 May 31;20(1):80. https://doi.org/10.1186/s13007-024-01213-3

60. Taks NW, Batstra MD, Kortekaas RF, Stevens FD, Pfeilmeier S, Van Den Burg HA. Non-Invasive, Bioluminescence-Based Visualisation and Quantification of Bacterial Infections in *Arabidopsis* Over Time. Mol Plant Pathol. 2025 Feb;26(2):e70055. https://doi.org/10.1111/mpp.70055

61. Lampropoulos A, Sutikovic Z, Wenzl C, Maegele I, Lohmann JU, Forner J. GreenGate-a novel, versatile, and efficient cloning system for plant transgenesis. PloS One. 2013;8(12):e83043. https://doi.org/10.1371/journal.pone.0083043

62. Clough SJ, Bent AF. Floral dip: a simplified method for Agrobacterium-mediated transformation of *Arabidopsis thaliana*. Plant J. 1998;16(6):735–43. https://doi.org/10.1046/j.1365-313x.1998.00343.x

63. Choi KH, Schweizer HP. mini-Tn7 insertion in bacteria with single attTn7 sites: example *Pseudomonas aeruginosa*. Nat Protoc. 2006 Jun 1;1(1):153–61. https://doi.org/10.1038/nprot.2006.24

64. Soldan R, Sanguankiattichai N, Bach-Pages M, Bervoets I, Huang WE, Preston GM. From macro to micro: a combined bioluminescence-fluorescence approach to monitor bacterial localization. Environ Microbiol. 2021 Apr;23(4):2070–85. https://doi.org/10.1111/1462-2920.15296

65. Bao Y, Lies DP, Fu H, Roberts GP. An improved Tn7-based system for the single-copy insertion of cloned genes into chromosomes of gram-negative bacteria. Gene. 1991;109(1):167–8. https://doi.org/10.1016/0378-1119(91)90604-A

66. Figurski DH, Helinski DR. Replication of an origin-containing derivative of plasmid RK2 dependent on a plasmid function provided in trans. Proc Natl Acad Sci. 1979;76(4):1648–52.

67. Kado CI, Heskett MG. Selective media for isolation of *Agrobacterium*, *Corynebacterium*, *Erwinia*, *Pseudomonas* and *Xanthomonas*. Phytopathology. 1970;60(6):969–76.

68. Atwell S, Huang YS, Vilhjálmsson BJ, Willems G, Horton M, Li Y, et al. Genome-wide association study of 107 phenotypes in *Arabidopsis thaliana* inbred lines. Nature. 2010;465(7298):627–31. https://doi.org/10.1038/nature08800

69. Zhang Z, Ersoz E, Lai CQ, Todhunter RJ, Tiwari HK, Gore MA, et al. Mixed linear model approach adapted for genome-wide association studies. Nat Genet. 2010;42(4):355–60. https://doi.org/10.1038/ng.546

70. Asai S, Cevik V, Jones JD, Shirasu K. Cell-specific RNA profiling reveals host genes expressed in *Arabidopsis* cells haustoriated by downy mildew. Plant Physiol. 2023;193(1):259–70. https://doi.org/10.1093/plphys/kiad326

71. Wu FH, Shen SC, Lee LY, Lee SH, Chan MT, Lin CS. Tape-Arabidopsis Sandwich - a simpler *Arabidopsis* protoplast isolation method. Plant Methods. 2009 Nov 24;5(1):16. https://doi.org/10.1186/1746-4811-5-16

Supporting information

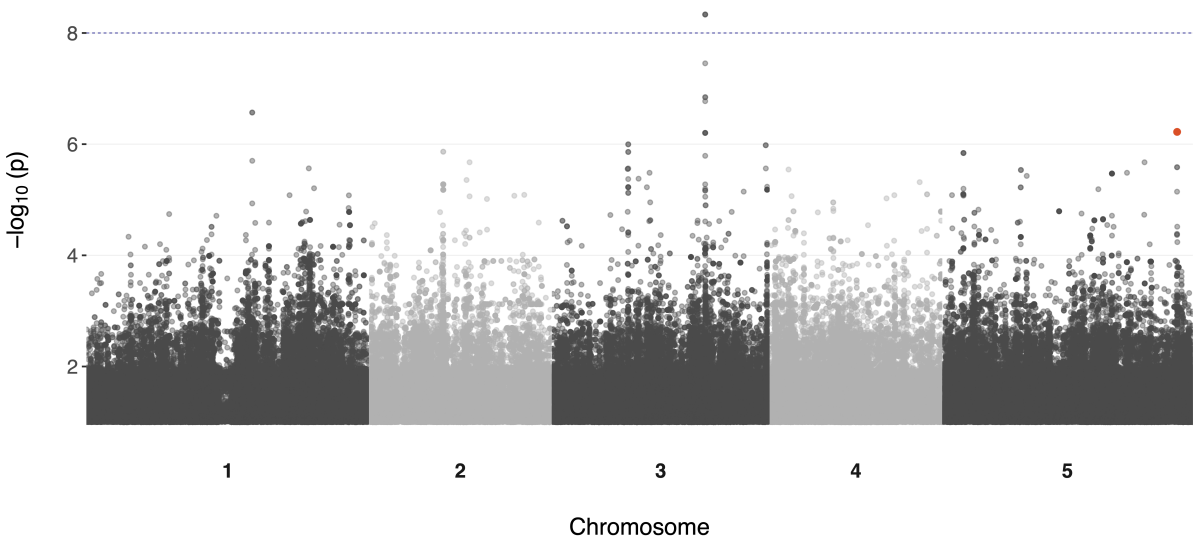

Figure S1. Manhattan plot of from a screen of 321 accessions present in the HapMap collection. Highlighted SNPs in orange are located within the coding sequence of *SUT1*. False Discovery Rate (FDR) threshold set at -$\log_{10}$ (p) = 8 (Bonferroni). Significantly correlated SNP on Chr 3 is located in the *LAS1* gene (AT3G45130).

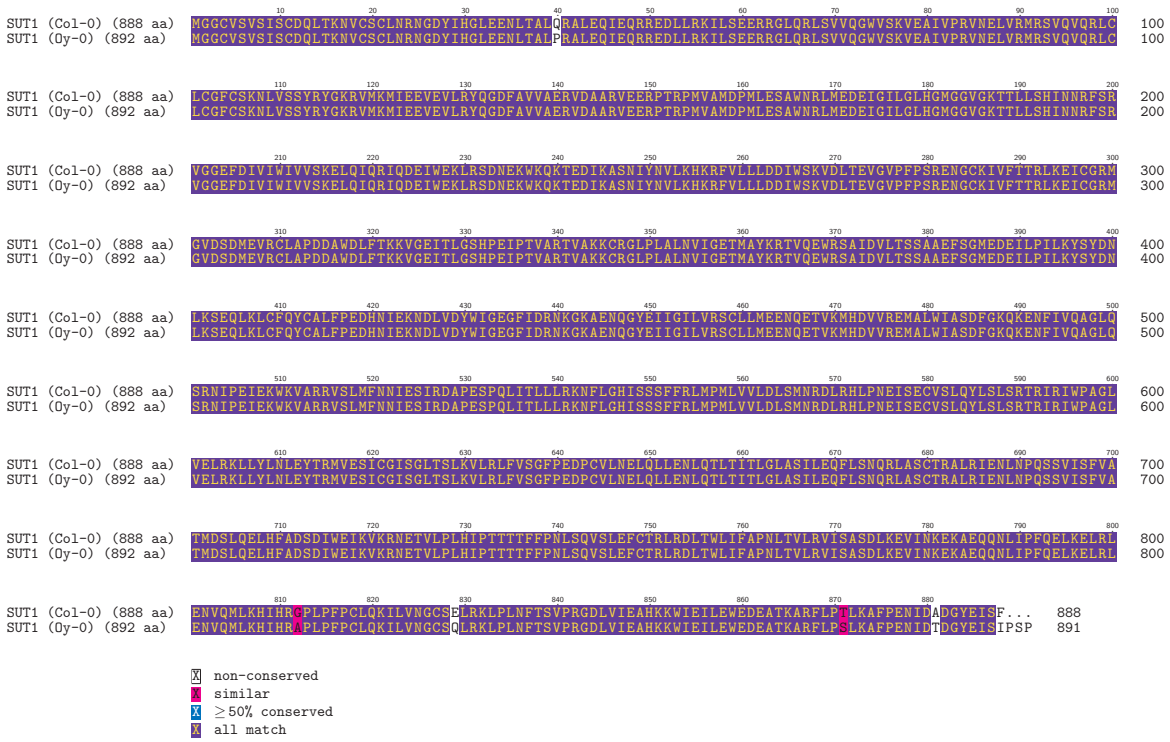

Figure S2. Alignment of predicted SUT1 protein sequences of the Arabidopsis accessions Col-0 and Oy-0. Coding sequences of *SUT1*$^{Col\text{-}0}$ and *SUT1*$^{Oy\text{-}0}$ were obtained from [32] and translated *in silico* into amino acid sequences. Alignment depicts six predicted amino acid substitutions in SUT1$^{Oy\text{-}0}$ compared to SUT1$^{Col\text{-}0}$, of which one is predicted to result in a 3-residue peptide extension at the C-terminus in SUT1$^{Oy\text{-}0}$.

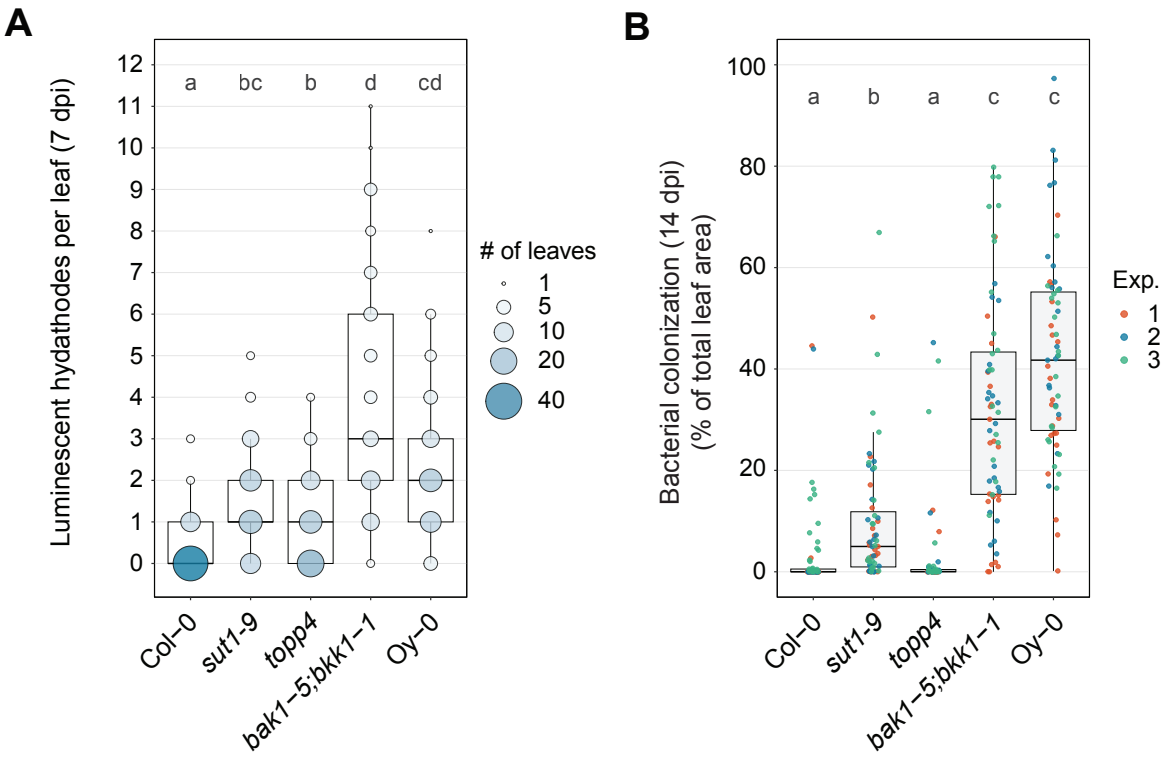

Figure S3. SUT1 resistance in Arabidopsis Col-0 does not depend on TOPP4 function. A) Number of infected hydathodes per leaf at 7 dpi following spray inoculation with Xcc8004 *ΔxopAC* Tn*7:lux*. Circles depict number of leaves for each score (n = 63 leaves per plant line). The *topp4* knockout shows a slight increase in hydathode infections compared to the Col-0 control. Significance letters from non-parametric Kruskal-Wallis test with Dunn's Post-Hoc test, p-value threshold = 0.05. **B)** Bacterial colonization defined as percentage of total leaf area colonized per leaf following spray inoculation with Xcc8004 *ΔxopAC* Tn*7:lux* (14 dpi, n = 21 leaves per experiment). Bacterial colonization was calculated using ScAnalyzer [59]. The *topp4* knockout does not display increased bacterial spread compared to the wildtype control (Col-0). Significance letters from non-parametric Kruskal-Wallis test with Dunn's Post-Hoc test, p-value threshold = 0.05.

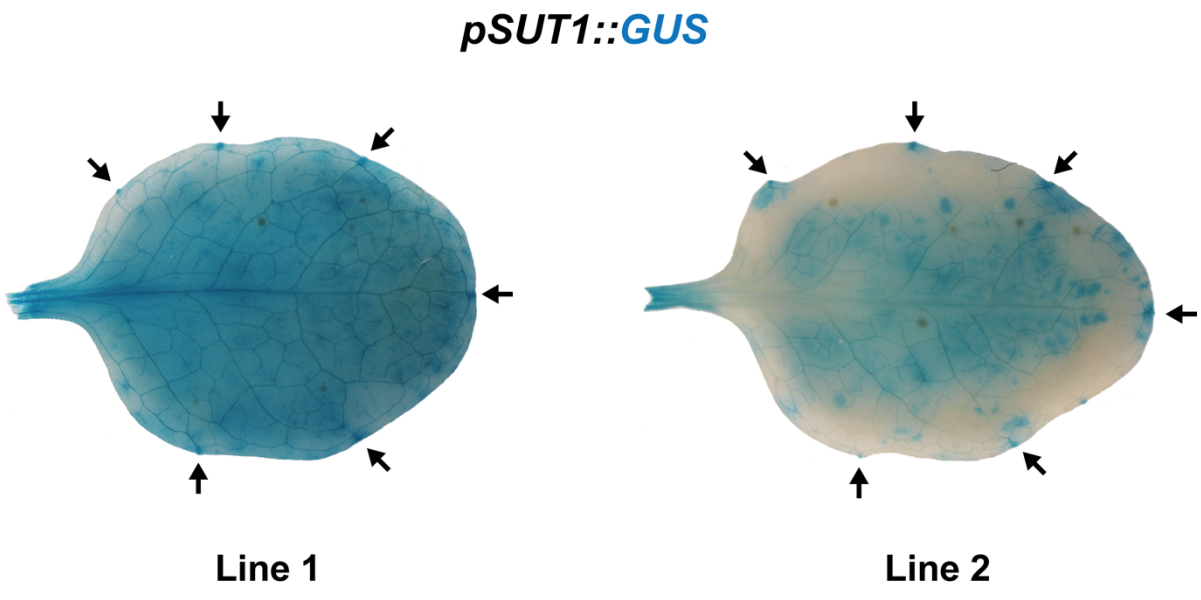

757

758 **Figure S4. *SUT1* is expressed in hydathodes and mesophyll.** Two independent homozygous T3 lines of 4-week-old

759 Arabidopsis *pSUT1::GUS* show GUS enzymatic activity in hydathodes (black arrows) and mesophyll tissue throughout

760 the leaf. Leaves were incubated in GUS staining solution for two hours.

761

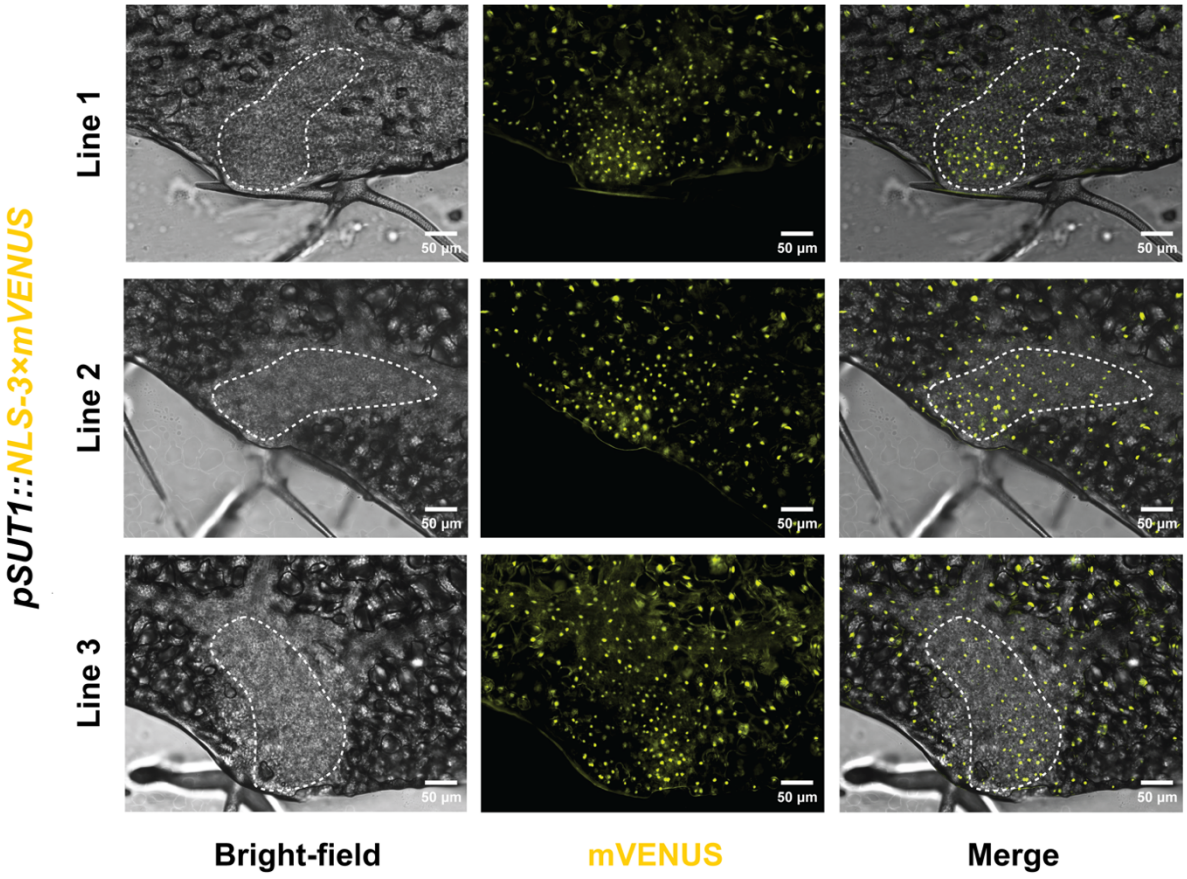

Figure S5. *SUT1* is expressed in epithem cells within hydathodes. Three independent T2 lines of 4-week-old Arabidopsis *pSUT1::NLS-3×mVENUS* show nuclear accumulation of mVENUS in the mesophyll and epithem. Epithem cells can be distinguished from mesophyll cells in the bright-field image as a cell dense area present on the leaf margin connected to the vasculature (white dashed line).

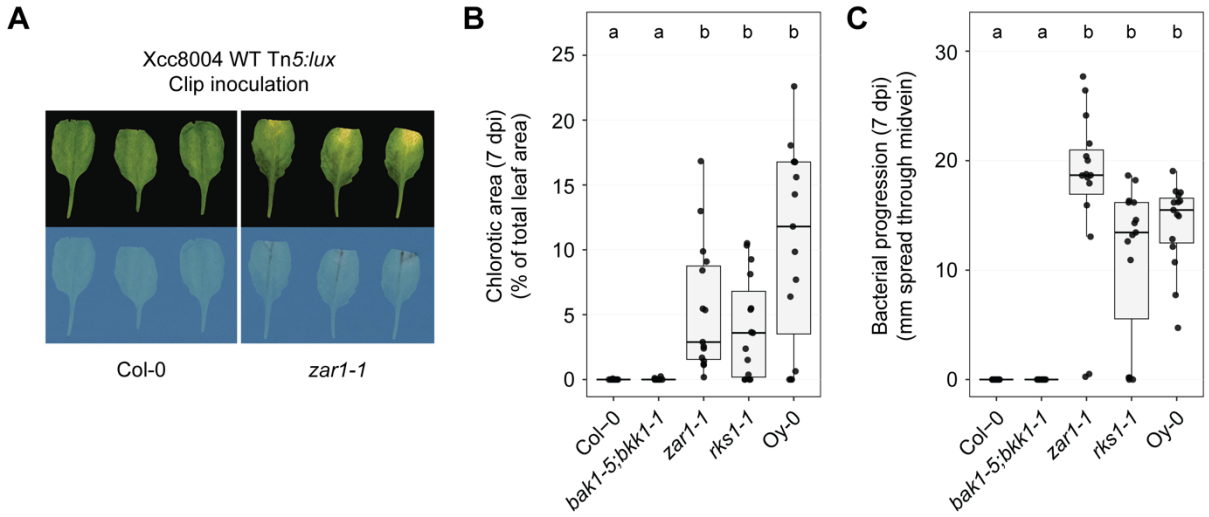

Figure S6. *RKS1/ZAR1* immunity against Xcc in the leaf vasculature. A) Disease symptoms and bacterial luminescence in resistant Col-0 and susceptible *zar1-1* knockout lines, 7 dpi following clip inoculation with Xcc8004 WT Tn*5:lux*. **B,C)** Chlorotic leaf area (**B**) and bacterial spread along the midvein (**C**) 7 dpi following clip inoculation with Xcc8004 WT Tn*5:lux* on Arabidopsis Col-0, *bak1-5;bkk1-1*, *zar1-1*, *rks1-1* and Oy-0 (n = 12 leaves). ZAR1-mediated resistance against Xcc is effective in the vasculature of Col-0 and *bak1-5;bkk1-1* when the hydathodes are bypassed and the bacteria are introduced using leaf clipping. Significance letters from a two-way ANOVA with Tukey Post-Hoc test, p-value threshold = 0.05.

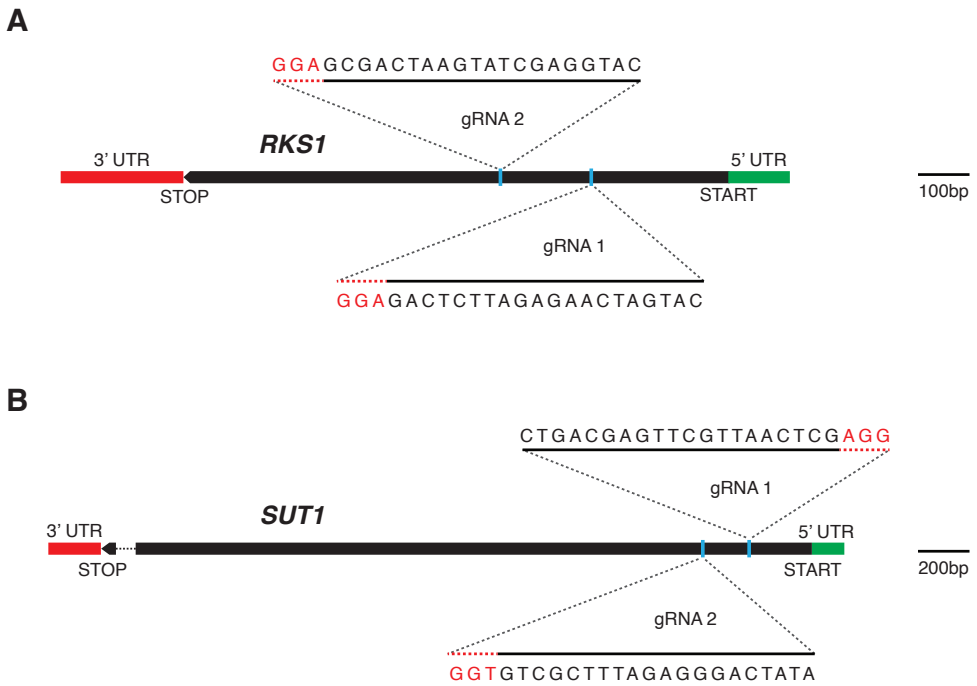

C

rks1/sut1 #1

RKS1	g1	GAGTAGGAGACNTCTTAGAGAACTAGTACATTCT	+1	**STOP** (93)
	g2	GTGGAGGAGCGACTAAGTATCGAGGTACAAGAC GTGGAGGAGCGNNACTAAGTATCGAGGTACAAGAC	+0/+2	NA
SUT1	g1	TCATTCTGACGAGTTCGTTAACTCGAGGTACTA	+0	NA
	g2	TCGGTGGTGTCNGCTTTAGAGGGACTATAGCTTC	+1	**STOP** (140)

rks1/sut1 #2

RKS1	g1	GAGTAGGAGACNTCTTAGAGAACTAGTACATTCT GAGTAGGAGACNNTCTTAGAGAACTAGTACATTCT	+1/+2	**STOP** (93)/ **STOP** (115)
	g2	GTGGAGGAGCGACTAAGTATCGAGGTACAAGAC GTGGAGGAGCGNNACTAAGTATCGAGGTACAAGAC	+0/+2	NA
SUT1	g1	TCATTCTGACGAGTTCGTTAACTCGAGGTACTA	+0	NA
	g2	TCGGTGGTGTCNGCTTTAGAGGGACTATAGCTTC	+1	**STOP** (140)

Figure S7. Confirmation of *rks1/sut1* double knockout mutants in Col-0 background. A,B) Schematic overview of two guide RNAs targeting the first exons of each target gene, *RKS1* (**A**) and *SUT1* (**B**), in Col-0. **C)** Schematic overview of resulting homozygous (when single sequence is shown) or biallelic (when two sequences are shown) indels (green N's) introduced at each gRNA target sode (g1 and g2) in two individual T1 mutant lines (#1 and #2). Both lines, *rks1/sut1* #1 and #2, show confirmed early STOP codons in both alleles of both target genes, as indicated on the right.

S1 Table. List of oligonucleotides, plasmids, plant lines and bacterial strains used in this study.

Extended data available at: *https://doi.org/10.21942/uva.28082129*

Extended Data 1. Raw data of RIL population genetic structure and disease scoring.

Extended Data 2. Raw data on disease scoring of HapMap population for GWAS.